BRAIN
ORIGINAL ARTICLE

Activation of α7 nicotinic acetylcholine receptor ameliorates HIV-associated neurology and neuropathology

Xiaojie Zhao,[1,2] Kelly Wilson,[1,2] Victor Uteshev[3] and Johnny J. He[1,2,4]

HIV-associated neurocognitive disorders (HAND) in the era of combination antiretroviral therapy are primarily manifested as impaired behaviours, glial activation/neuroinflammation and compromised neuronal integrity, for which there are no effective treatments currently available.

In the current study, we used doxycycline-inducible astrocyte-specific HIV Tat transgenic mice (iTat), a surrogate HAND model, and determined effects of PNU-125096, a positive allosteric modulator of α7 nicotinic acetylcholine receptor (α7 nAChR) on Tat-induced behavioural impairments and neuropathologies.

We showed that PNU-125096 treatment significantly improved locomotor, learning and memory deficits of iTat mice while inhibited glial activation and increased PSD-95 expression in the cortex and hippocampus of iTat mice. Using α7 nAChR knockout mice, we showed that α7 nAChR knockout eliminated the protective effects of PNU-125096 on iTat mice. In addition, we showed that inhibition of p38 phosphorylation by SB239063, a p38 MAPK-specific inhibitor exacerbated Tat neurotoxicity in iTat mice. Last, we used primary mouse cortical individual cultures and neuron-astrocytes co-cultures and *in vivo* staining of iTat mouse brain tissues and showed that glial activation was directly involved in the interplay among Tat neurotoxicity, α7 nAChR activation and the p38 MAPK signalling pathway.

Taken together, these findings demonstrated for the first time that α7 nAChR activation led to protection against HAND and suggested that α7 nAChR modulator PNU-125096 holds significant promise for development of therapeutics for HAND.

1 Department of Microbiology and Immunology, Rosalind Franklin University, Chicago Medical School, North Chicago, IL 60064, USA
2 Center for Cancer Cell Biology, Immunology and Infection, Rosalind Franklin University, North Chicago, IL 60064, USA
3 Department of Pharmacology and Neuroscience, Graduate School of Biomedical Sciences of University of North Texas Health Science Center, Fort Worth, TX 76107, USA
4 School of Graduate and Postdoctoral Studies, Rosalind Franklin University, North Chicago, IL 60064, USA

Correspondence to: Johnny J. He, PhD
Department of Microbiology and Immunology
Rosalind Franklin University, Chicago Medical School
3333 Green Bay Road, North Chicago, IL 60064, USA
E-mail: johnny.he@rosalindfranklin.edu

Keywords: α7 nAChR; PAM; HIV Tat; HAND; p38 MAPK

Received January 17, 2021. Revised March 28, 2021. Accepted June 3, 2021. Advance access publication July 1, 2021

Abbreviations: DMSO = dimethyl sulphoxide; HAND = HIV-associated neurocognitive disorders; iTat = doxycycline-inducible and astrocyte-specific HIV Tat transgenic mice; nAChR = nicotinic acetylcholine receptor; p38 MAPK = p38 mitogen-activated protein kinase; PAM = positive allosteric modulator

Introduction

Combination antiretroviral therapy (cART) has effectively suppressed HIV replication and improved immune function as well as prolonged the lifespan of individuals infected with HIV.[1–5] However, HIV-associated neurocognitive disorders (HAND) have become more prevalent. The neurological manifestations include slowed locomotor activity, impaired learning and memory, and the neuropathological hallmarks are astrocyte/microglia activation, chronic neuroinflammation and comprised neuronal integrity.[6–15] None of antiretrovirals that are used in the current cART regimens have shown significant penetrance into the CNS and have provided effective treatments for HAND.[16–19]

HIV viral protein Tat is a major pathogenic factor for HAND. It is secreted from HIV-infected microglia and astrocytes and taken up by neurons,[20–24] and detected in the brain of HIV-infected individuals who are cART naïve and who are actively treated with cART.[25–27] Tat expression activates glial fibrillary acidic protein (GFAP) expression in astrocytes through a cascade of transcription factors such as STAT3, early growth response 1 and p300 and causes astrocyte dysfunction and decreases neuron survival.[28–32] In addition, Tat expression alters autophagy, endoplasmic reticulum stress, lysosomal exocytosis, neurite growth and neurogenesis.[33–37] Importantly, Tat expression in the brain of doxycycline-inducible astrocyte-specific HIV Tat transgenic mice (iTat) in the absence of HIV infection leads to locomotor, learning and memory deficits,[38–46] and astrocyte/microglia activation, chronic neuroinflammation and loss of neuronal integrity,[30,38,41,45] the consistent neurological and neuropathological hallmarks of HAND in the era of cART.

Nicotinic acetylcholine receptors (nAChR) are expressed throughout the PNS and CNS, and they respond/bind to the endogenous agonist neurotransmitter acetylcholine or the exogenous agonist drug nicotine.[47,48] One of the most abundant nAChR is homomeric α7 nAChR, which is both ionotropic and metabotropic and is predominantly expressed in neurons and glia of cortex and hippocampus.[49,50] The ionotropic feature of α7 nAChR is the fast desensitization rate, characterized by very short agonist-induced onset duration and rapid decay with a long-lasting desensitized state.[50] The metabotropic feature is related to M3-M4 intracellular loop,[51] which involves multiple cellular signalling pathways including MAPK, PLC-RhoA, JAK2-STAT3 and PI3K-Akt and modulates synaptogenesis and growth in neural cells and inflammatory response in immune cells.[52–60] α7 nAChR is involved in several neurological disorders such as Alzheimer's disease,[49] schizophrenia,[61] drug addiction,[62,63] depression[64] and pain.[65] It has been proposed as a potential therapeutic target for Alzheimer's disease,[49] addiction,[66] schizophrenia,[66,67] ischaemic[68] and traumatic brain injury.[69] α7 nAChR has also been shown to be involved in HIV gp120 and gp41 neurotoxicity.[70–72] However, little is known about its roles in HAND and its potential as a therapeutic target for treating HAND.

In the current study, we aimed to determine the roles of α7 nAChR in HAND. We took advantage of PNU-120596, a prototype-II and highly selective α7 nAChR positive allosteric modulator (PAM),[50,73–75] and the surrogate HAND model iTat mice and determined whether PAM PNU-120596 treatment would lead to any changes in Tat-induced behavioural impairments and neuropathologies. In addition, we used α7 nAChR knockout mice and determined the direct roles of α7 nAChR in Tat neurotoxicity. Furthermore, we determined whether and which mitogen-activated protein kinase (MAPK) signalling pathway(s) were involved in the interplay between Tat neurotoxicity and α7 nAChR activation. Finally, we used individual primary mouse cortical cultures and neuron-astrocytes co-cultures and assessed the relative contribution of neurons, astrocytes and microglia to the interplay among Tat neurotoxicity, α7 nAChR activation and p38 MAPK signalling pathway.

Materials and methods

Mouse and drug administration

We generated iTat mice as previously described.[38] Wild-type (C57BL/6) and α7 nAChR knockout mice ($\alpha7^{-/-}$, B6.129S7-Chrna$^{7tm1Bay/J}$) were purchased from the Jackson Laboratory. All the animal procedures were approved by the Institutional Animal Care and Use Committee. Mice were housed with a 12-h light and 12-h dark photoperiod and provided water and food *ad libitum*. $\alpha7^{-/-}$iTat mice were generated by cross-breeding iTat mice with $\alpha7^{-/-}$ mice. $\alpha7^{-/-}$ genotyping was slightly modified with the JumpStart™ Taq DNA Polymerase-based PCR (JumpStart Taq DNA Polymerase, Sigma, Cat no. D9307). Briefly, genomic DNA was extracted from the mouse tail and used a template for PCR with a program of 94°C for 1 min, 35 cycles of 94°C for 30 s, 55°C for 30 s, and 72°C for 1 min, and one cycle of 72°C for 1 min using primers 5′-TTC CTG GTC CTG CTG TGT TA-3′ and 5′-ATC AGA TGT TGC TGG CAT GA-3′ for $\alpha7^{+/+}$ wild-type mice, and 5′-TTC CTG GTC CTG CTG TGT TA-3′ and 5′-CCC TTT ATA GAT TCG CCC TTG-3′ for $\alpha7^{-/-}$ knockout mice. Mice aged 10–14 weeks with body weights of 20–35 g were fed a doxycycline-containing diet (0.625 g/kg, Envigo, Cat no. TD.01306) as stated. PNU-120596 hydrate (Alomone, Cat no. P-350) was dissolved in dimethyl sulphoxide (DMSO) and subcutaneously (s.c.) injected (15 mg/kg/day, 40 μl for male mice with an average weight of 30 g and 30 μl for female mice with an average weight of 22 g to ensure minimal DMSO-associated toxicity).[76] SB239063 (Tocris, Cat no. 1962) was dissolved first in 100% DMSO and mixed with PEG400 (Sigma-Aldrich, Cat no. 91893) and saline at a ratio of 0.8:32:67, then intraperitoneally (i.p.) injected (15 mg/kg/day, 200 μl for male mice and 150 μl for female mice).[77]

Behavioural tests

The open field test and Morris water maze were performed sequentially using a computerized video tracking system (ANY-maze, Stoelting) to determine the spontaneous locomotor activity and spatial learning and memory, respectively. For the open field test, each mouse was allowed to move freely around a clear acrylic chamber (40.5 × 40.5 × 30.5 cm) for 10 min. Travel distance and maximum speed were determined by the ANY-maze software. For the Morris water maze, a circle pool (1.2 m in diameter) surrounded with a curtain was divided into four equal quadrants, and four

signs with different shape were fixed onto the middle of each quadrant wall above the opaque water (24 ± 1°C). A hidden platform (1.5 cm below water surface) was put into a certain quadrant. Two stages consisting of 5-day training and probe test were carried out. In the training stage, four trials with a 15–20 min interval were conducted in the every day training, and for each trial mice were allowed to freely seek the platform within 90 s right after they were randomly put into one quadrant facing to the pool wall. If the mice found the platform within 90 s, 10 s would be added to allow them staying on the platform for memorizing; however, if they failed, they would be directed towards the platform and allowed to stay on it for 15 s. Mice that were immobile or floating and unable to find the platform during the training stages were excluded from the experiments. Probe test was carried out on the next day following the 5-day training stage with a 60 s trial, and the platform was removed to prevent the mice from climbing onto it during the testing. One day after the behavioural tests, mice were euthanized and the brains were harvested.

Western blotting

A RIPA buffer (50 mM Tris.HCl, pH 8.0, 280 mM NaCl, 0.5% NP-40, 1% $C_{24}H_{39}NaO_4$, 0.2 mM EDTA, 2 mM EGTA and 10% glycerol) supplemented with protease inhibitors (Millipore-Sigma, Cat no. S8830) and phosphatase inhibitors (Millipore-Sigma, Cat no. 4906845001) was used to lyse the brain tissues and cultured cells with brief sonication on ice. Protein concentrations of the lysates were determined using a Bio-Rad DC protein assay kit (Bio-Rad, Cat no. 5000111). Lysates were denatured in the SDS-PAGE loading buffer at 100°C for 10 min, then electrophoretically separated by 8–15% SDS–PAGE, blotted onto 0.45-μm polyvinylidene fluoride membrane (GE Healthcare Life Sciences, Cat no. 10600023) and probed using appropriate antibodies against PSD-95 (Abcam, Cat no. ab18258 and 1:2000 dilution), SYP (Abcam, Cat no. ab8049 and 1:1000 dilution), Iba-1 (Wako, Cat no. 016–20001 and 1:500 dilution) and GFAP (DAKO, Cat no. z330s and 1:2000 dilution), p-p38 (Santa Cruz, Cat no. sc-166182 and 1:1000 dilution), p38 (Santa Cruz, Cat no. sc-535 and 1:1000 dilution), p-JNK (Santa Cruz, Cat no. sc-6254 and 1:1000 dilution), JNK (Santa Cruz, Cat no. sc-571 and 1:1000 dilution), p-ERK (Santa Cruz, Cat no. sc-7383 and 1:1000 dilution), and ERK (Santa Cruz, Cat no. sc-514302 and 1:1000 dilution), α7 nAChR (Alomone, Cat no. ANC-007 and 1:1000 dilution) and β-actin (Sigma-Aldrich, Cat no. A1978 and 1:2000 dilution). A Bio-Rad ChemicDoc imaging system (Bio-Rad) and ImageJ were used for image capturing and analysis, respectively.

3′-Diaminobenzidine staining

Mice were anaesthetized using Avertin (tribromoethanol) and transcardially perfused with first PBS and then 4% paraformaldehyde (PFA). Next, the brains were dissected out, fixed in 4% PFA at 4°C overnight, dehydrated in 30% sucrose, embedded in OCT, sagittally sectioned (20 μm) using a cryostat and preserved in a cryoprotectant containing 30% ethylene glycol, 30% glycerol and 40% PBS. For staining, floating sections were permeabilized in 0.1% Triton™ X-100 in PBS (PBST), blocked by 1% BSA in PBST, probed by Iba-1 antibody (Wako, Cat no. 019-19741 and 1:800 dilution), placed in inactivated endogenous peroxidases in 1% hydrogen peroxide, probed again by a goat anti-rabbit secondary antibody (SouthernBiotech, Cat no. 4030-05 and 1:200 dilution) and developed using a DAB kit (Abcam, Cat no. ab103723). All images were taken using a Nikon Eclipse E800 microscope with a 20× objective and analysed using the Cellprofiler program. Every section was averaged from three brain regions, the prefrontal, occipital and parietal cortex, and the average of the three sections was used to represent individual animals.

Preparation of primary mouse cortical neurons, microglia, astrocytes, neuron-astrocyte co-cultures

All primary cells were prepared from 1-day-old $\alpha7^{-/-}$ pups and their isogenic wild-type pups.

Primary cortical neurons

One-day-old pups were genotyped, the brains with desired genotypes were harvested, meninges removed and cortex dissected out. The cortex was minced in a cold Hanks' balanced salt solution (HBSS buffer, Sigma-Aldrich, Cat no. 55021C). HBSS buffer was replaced sequentially by 0.25% trypsin (Sigma-Aldrich, Cat no. T4049), 2 μg/ml deoxyribonuclease I (Sigma-Aldrich, Cat no. D5025) (at 37°C for 20 min), foetal bovine serum (2 min), 2% B27 (ThermoFisher, Cat no. 17504044) Neurobasal™ medium (ThermoFisher, Cat no. 21103049) and 1% GlutaMAX™ (ThermoFisher, Cat no. 35050061). Brief centrifugation (300*g*, 1–5 min) was used to recover the tissues and cells. The tissues were then triturated using a 10-ml pipette, the disassociated cells were washed and seeded into a 24-well plate (0.25 M/well), which was either coated with or contained coverslips coated with 0.1% poly-D-lysine (Sigma-Aldrich, Cat no. P6407) in borate buffer (pH 8.5), cultured at a 37°C, placed in a 5% CO_2 incubator for 2 days and treated with 2.5 μM cytosine β-D-arabinofuranoside (Ara-C, Sigma-Aldrich, Cat no. C1768) to remove astrocytes. Medium change by 50% was performed every 2 days and the neurons were ready for use on Day 12 with purity above 90%, estimated by MAP2 staining (Santa Cruz, Cat no. sc-32791 and 1:500 dilution).

Primary cortical neuron-astrocyte co-cultures

A similar protocol was used to generate primary cortical neuron-astrocyte co-cultures except for omission of the Ara-C treatment from the protocol. The ratio of neurons to astrocytes in the co-cultures was estimated to be 1.5–2:1, estimated by MAP2 and GFAP staining (1:500 dilution with the same antibodies for western blotting).

Primary cortical microglia and astrocytes

A similar protocol was used to generate primary microglia and astrocytes except for use of full Dulbecco's modified Eagle medium (DMEM, Corning, Cat no. MT15013CM) in place of B27 Neurobasal medium, which was used to allow glia to grow. All cells were seeded into a T-75 flask without coating. Once the cells reached confluence, which usually took 12–14 days for brain extraction of two pups, the flask was shaken around 200 rpm for 2 h to dislodge microglia. The culture medium containing the microglia was transferred to a 12-well plate, incubated in a 37°C, 5% CO_2 incubator for 30 min to allow the microglia to attach to the bottom of the well, and replaced with 20% LADMAC conditioned medium (see next) and 80% full DMEM, then cultured for 3–4 days with medium change every other day. The leftover astrocytes attached to the T-75 flasks were trypsinized, seeded into a 12-well plate and cultured in full DMEM for 3–4 days. The purity of microglia and astrocytes was greater than 99% as determined by staining for Iba-1 (the same antibody as the DAB staining) and GFAP, respectively.

Preparation of conditioned media and use in primary cell cultures

LADMAC conditioned medium

LADMAC cells (ATCC, Cat no. CRL-2420™) were cultured in a T-75 flask with EMEM (ATCC, Cat no. 30–2003), 10% foetal bovine serum

and 1% penicillin and streptomycin for 5–7 days to reach confluence. Then, the culture medium was collected, cell debris removed by brief centrifugation (300*g*, 5 min) and filtered (0.22 μm filter, SIMSII, Cat no. S30PES022S), then saved as LADMAC conditioned medium.

Tat-containing or control DMEM conditioned media

The 293T (ATCC, Cat no. CRL-3216™) cells were seeded into a 10 cm dish, cultured in DMEM containing 10% FBS, 1% penicillin and streptomycin for 24 h, transfected with 20 μg of pcDNA3-Tat.Myc by calcium phosphate precipitation, cultured for 24 h, changed for fresh DMEM medium and cultured for an additional 48 h. Then the culture medium was collected, cell debris removed by centrifugation (300*g*, 5 min) followed by filtering through a 0.22-μm filter and saved as Tat-containing conditioned medium (Tat-CM). As a control, pcDNA3 was also transfected in order to generate the control condition medium (Ctrl-CM). To treat primary microglia, 70% Tat-containing or control conditioned medium, 20% fresh DMEM and 10% LADMAC conditioned medium were used. To treat primary astrocytes, 70% Tat-containing or control conditioned medium and 30% fresh DMEM were used.

Tat-containing or control neurobasal conditioned medium

The Tat-containing and control neurobasal conditioned medium was similarly prepared except for use of an increased number of seeding cells, 48 h culturing after transfection, change to neurobasal medium with 1% GlutaMAX™, then 24 h after the medium change and saved as Tat-containing neurobasal conditioned medium (Tat-CM) or control neurobasal conditioned medium (Ctrl-CM). To treat primary neurons and primary cortical neuron-astrocyte co-cultures, 98% Tat-containing or control neurobasal conditioned medium and 2% B27 (50×) were used to replace the 50% culture medium. To activate α7 nAChR in cell cultures, 1 μM PNU-120596 accompanied with 0.5 μM PNU-282987 (Sigma-Aldrich, Cat no. P6499) (PAM+P2) was applied into the conditioned medium. Both of them were dissolved in DMSO at high concentrations (PNU-120596: 100 mM, PNU-282987: 50 mM) as stocks. A Nikon Eclipse TE2000-S microscope with a 10× objective was used to capture the images of microglia in the bright field, and the images were converted using the Ilastik program to visualize the cell morphology, and then were quantitated by the Cellprofiler program. Three images were randomly captured from each well.

Immunofluorescence staining

Brain sections (20 μm) were permeabilized in PBST, blocked in 1% BSA in PBST and probed using appropriate primary antibodies against PSD-95 (1:500 dilution with the same western blotting antibody) or MAP2 (same to above) and secondary antibodies goat anti-rabbit 555 (ThermoFisher, Cat no. A21428 and 1:500 dilution) or goat anti-mouse 488 (ThermoFisher, Cat no. A11001 and 1:500 dilution). For cultured cells, the cells were first fixed with 4% PFA for 10 min, and then we proceeded using the same procedures as for the brain sections. All images from brain sections were taken using Olympus FV10i confocal microscope with a 60× oil objective. The entire cortex and hippocampus region were checked, and frontal cortex and CA1 were chosen as the representative regions to verify PSD-95 expression. All culture cell images were taken using a Nikon Eclipse 800 microscope with a 100× oil objective. Three to six individual neurons were randomly selected and averaged for each coverslip. PSD-95-positive puncta within the trunk of neuron dendrites (first order) was analysed for primary cortical neurons, while PSD-95-positive puncta of the secondary dendrites (second order) were analysed for neuron-astrocyte co-cultures. ImageJ was used to determine the percentage of PSD-95 positive area to the total MAP2-positive area.

Data analysis

Three-way repeated measures ANOVA was used in MWZ training stages, and all other experiments used either two- or three-way ANOVA, whenever applicable. The Bonferroni test was used for all *post hoc* analyses. All statistical analyses were performed using IBM SPSS 20. $P < 0.05$ was considered significant and indicated with an asterisk, number symbol or dollar sign for comparisons among different groups; $^{**}P < 0.01$ and $^{***}P < 0.001$ were both considered highly significant and are indicated with asterisks.

Data availability

All raw data that were presented or mentioned in the manuscript are available from the corresponding author on request.

Results

PAM administration alleviated HIV Tat-induced behavioural deficits and neuropathologies

To determine whether α7 nAChR is involved in HAND, iTat mice were fed with doxycycline-containing food pellets for 7 days, injected subcutaneously with PNU-120596, a well-studied and highly specific PAM of α7 nAChR[73,74] for 5 days, and then subjected to an open field test for locomotor activity on Day 14 and the Morris water maze test for learning and spatial memory on Days

Table 1 Experimental groups for PAM treatment, α7 nAChR knockout with PAM treatment and p38 MAPK inhibitor

Mice	Sex	PAM treatment[a]	α7 genotype[b]	p38 MAPK inhibitor
Wild-type	Male	WT+DMSO	$\alpha7^{+/+}$WT	WT+Vehicle[c]
		WT+PAM	$\alpha7^{-/-}$WT	WT+SB239063
	Female	WT+DMSO	$\alpha7^{+/+}$WT	WT+Vehicle
		WT+PAM	$\alpha7^{-/-}$WT	WT+SB239063
iTat	Male	WT+DMSO	$\alpha7^{+/+}$iTat	iTat+Vehicle
		WT+PAM	$\alpha7^{-/-}$iTat	iTat+SB239063
	Female	WT+DMSO	$\alpha7^{+/+}$iTat	iTat+Vehicle
		WT+PAM	$\alpha7^{-/-}$iTat	iTat+SB239063

WT = wild-type.
[a]PAM was dissolved in 100% DMSO and DMSO was used as the control.
[b]$\alpha7^{+/+}$ = wild-type α7 nAChR knockout; $\alpha7^{-/-}$ = α7 nAChR knockout. All animals in this experiment were treated with PAM.
[c]Vehicle: p38 MAPK inhibitor SB239063 was dissolved in 100% DMSO, then diluted in PEG400 and saline in a ratio of 0.8:32:67. Thus, vehicle was a mix of DMSO, PEG400 and saline at a 0.8:32:67 ratio.

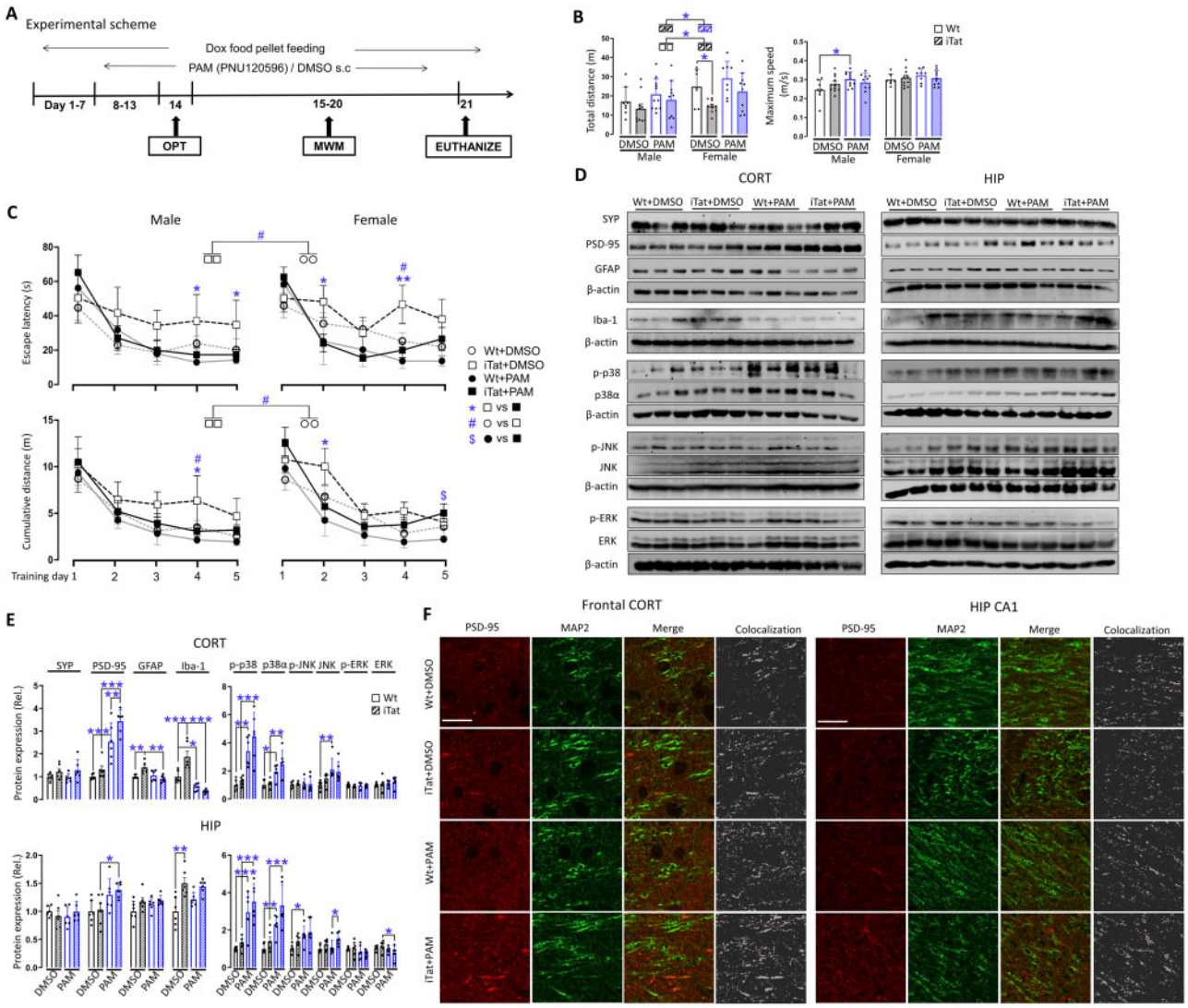

Figure 1 Effects of PAM on HIV-1 Tat-induced behavioural impairments and neuropathologies. (**A**) Wild-type (Wt) or iTat mice 3–4 months of age were fed with doxycycline (Dox)-containing food pellets and injected subcutaneously (s.c.) with PAM PNU-125096 (15 mg/kg/day) or its solvent DMSO control, and grouped by sex (n = 6–11/group). The mice were subject to an open field test (**B**) and Morris Water Maze test (training stage, **C**), and the behavioural indices were determined by the ANY-maze software. During the behavioural tests, doxycycline-containing food pellet feeding continued *ad libitum*, PNU-125096 was administrated within 5 h following each behavioural test. (**D**) On Day 21, 1 day after the last behavioural test, all mice were euthanized, cortex (CORT) and hippocampus (HIP) were dissected out to determine expression of synaptophysin (SYP), PSD-95, GFAP and Iba-1, and total and phosphorylated p38, JNK and ERK by western blotting. (**E**) Protein expression was quantified by densitometry and normalized to the loading control β-actin and calculated using Wt+DMSO as a reference, which was set at 1 (n = 6/group, three males and three females). (**F**) Immunofluorescent staining was performed for PSD-95 and MAP2 expression. Scale bars = 20 μm. Subregions in frontal cortex and hippocampus CA1 were chosen as representative region for the cortex and hippocampus, respectively. $P < 0.05$ was considered significant and is indicated with asterisk, number symbol or dollar sign for comparisons among different groups; $^{**}P < 0.01$ and $^{***}P < 0.001$ were both considered highly significant and are indicated with asterisks.

15–20, before being euthanized to harvest tissues on Day 21 (Fig. 1A). Doxycycline-containing food pellet feeding and PAM injection continued during the next 7 days of behavioural tests. To minimize the effects of injection on behavioural tests, PAM was injected 5 h after each behavioural test. Wild-type mice and solvent DMSO were included as controls for iTat mice and PAM in the experiments, respectively, and mice were further grouped by sex, which gave rise to a total of eight experimental groups for analyses (Table 1).

For the open field test, the total travel distance and the maximum speed were measured. In DMSO treatments, iTat mice showed a shorter travel distance than wild-type mice for both male and female mice, and the difference between the female iTat mice and female wild-type was much greater than the difference between male iTat mice and female wild-type mice (Fig. 1B, left). In comparison, PAM treatment led to improvement in the travel distance of iTat mice and some improvement in the travel distance of wild-type mice. For maximum speed, there was no difference between iTat mice and wild-type mice in the DMSO treatment group, and PAM treatments led to increases in the maximum speed of male wild-type mice but not for the others (Fig. 1B, right).

At the Morris water maze training stage, escape latency time ('escape latency') and cumulative travel distance ('cumulative

distance') were measured. Compared to wild-type mice treated with DMSO, iTat mice treated with DMSO showed a longer escape latency time (Fig. 1C, top left) and longer cumulative travel distance (Fig. 1C, bottom) on all 5 days, with differences of cumulative travel distances in male mice and escape latency time for female mice on Day 4. PAM treatment led to remarkable improvements in iTat mice, with differences of escape latency time in male iTat mice on Days 4 and 5 and female iTat mice on Days 2 and 4 (Fig. 1C, top), and differences of cumulative travel times in male iTat mice on Day 4 and female iTat mice on Day 2 (Fig. 1C, bottom). However, only some improvements in male wild-type mice were found by PAM treatment. In addition, there was an increase in cumulative travel distance in PAM-treated female iTat mice on Day 5 when compared with PAM-treated female wild-type mice.

For the Morris water maze probe test, latency to the platform, platform entries, time at target quadrant, distance to target quadrant, time at the platform and distance to the platform were measured. Male iTat mice treated with DMSO showed less time at target quadrant and shorter distance to target quadrant, which were reversed by PAM treatment with the differences in distance to target quadrant (Supplementary Fig. 1, middle). Interesting to note is the longer latency to the platform in male iTat mice treated with DMSO than male wild-type mice treated with DMSO, and decreases of latency to the platform in both male iTat and wild-type mice by PAM treatment (Supplementary Fig. 1, left). For other indices including platform entries, time at the platform and distance to the platform, there were no differences between iTat and wild-type mice, DMSO- and PAM-treated mice, and male and female mice.

We next determined the changes of neuron presynaptic synaptic marker synaptophysin (SYP) and postsynaptic marker PSD-95, astrocyte marker GFAP and microglia marker Iba-1 in cortex and hippocampus. In cortex, iTat mice treated with DMSO showed significantly higher GFAP and Iba-1 than wild-type mice treated with DMSO (right panels, Fig. 1D, right and E, top and left). PAM treatment led to significant increases of PSD-95 in wild-type mice and even more in iTat mice but had decreased GFAP in iTat mice and decreased Iba-1 in both wild-type and iTat mice. Meanwhile, SYP showed no changes between iTat mice and wild-type mice, and between DMSO and PAM treatment (Fig. 1D, right and E, top and left). In hippocampus, PAM treatment increased PSD-95 in both wild-type and iTat mice, and iTat mice treated with DMSO showed more Iba-1 than wild-type mice treated with DMSO (left panels, Fig. 1D, left and E, bottom and left). There were no differences of SYP and GFAP between wild-type mice and iTat mice, and between DMSO- and PAM-treated mice. PSD-95 expression and its location in all these tissues were further confirmed by double immunofluorescent staining for PSD-95 and MAP2 (Fig. 1F).

We next determined whether and which MAPK signalling pathways were responsive to PAM neuroprotective effects against Tat-induced neuropathologies. Both cortex and hippocampus were analysed for expression and phosphorylation of p38, JNK and ERK. PAM treatment led to increases of both p38 and p-p38α in both cortex and hippocampus, increases of JNK in cortex of wild-type mice, increases of JNK in cortex of iTat mice, increases of JNK and p-JNK in hippocampus of all mice and decreases of ERK in hippocampus of iTat mice (Fig. 1D right and E). PAM treatment also led to increases of JNK and p-JNK in both cortex and hippocampus of wild-type mice. There was a difference of JNK between PAM-treated iTat mice and PAM-treated wild-type mice. But there were no differences of p-JNK in cortex of all mice and no differences of p-ERK in cortex and hippocampus of both iTat and wild-type mice. Interestingly, iTat mice showed no changes in p38, JNK, ERK and their phosphorylated counterparts compared to wild-type mice, both in the absence and presence of PAM treatment. Furthermore, no differences were noted between female and male mice in all the molecular analyses, thus the data were pooled after normalization using wild-type mice treated with DMSO as the reference.

Taken together, we showed that PAM treatment significantly increased locomotor activity, enhanced learning and memory processes, elevated PSD-95 expression and inhibited GFAP and Iba-1 expression in iTat mice. We also showed that these changes were associated with increased levels of p38 and its phosphorylation, to a lesser extent JNK and its phosphorylation, but not ERK and its phosphorylation. All these changes were more pronounced in cortex of iTat mice than hippocampus of iTat mice. These findings demonstrated that PAM was neuroprotective against HIV Tat-induced behavioural impairments and neuropathologies, and suggest that PAM-mediated activation of α7 nAChR is probably involved.

α7 nAChR knockout abrogated PAM-induced neuroprotective function against Tat-induced behavioural impairments and neuropathologies

To ascertain the neuroprotective function of PAM and the roles of α7 nAChR in PAM neuroprotective function against Tat-induced behavioural impairments and neuropathologies, we cross-bred α7 nAChR knockout mice ($\alpha7^{-/-}$) with iTat mice, generated $\alpha7^{-/-}$iTat mice and used these mice in the subsequent three-way ANOVA design studies (α7 nAChR, iTat and sex; Table 1), in which all eight groups of mice were fed with doxycycline-containing food pellets and subcutaneously injected with PAM in the same way as stated in Fig. 1A and subject to the same behavioural tests and analysis of SYP, PSD-95, GFAP, Iba-1 and MAPK signalling pathways.

In the open field test, there were only differences of total travel distance and maximum speed between wild-type $\alpha7^{-/-}$ ($\alpha7^{-/-}$WT) female mice and $\alpha7^{-/-}$iTat female mice (Fig. 2A). During the Morris water maze training stage, $\alpha7^{-/-}$iTat male mice showed longer escape latency than $\alpha7^{+/+}$iTat male mice on all 5 days with differences on Days 2 and 3 (Fig. 2B, top left). $\alpha7^{-/-}$iTat male mice also had longer cumulative travel distance than $\alpha7^{+/+}$iTat male mice on Day 3 (Fig. 2B, bottom left). All female mice showed no differences in escape latency and cumulative distance (Fig. 2B, right). In addition, compared with $\alpha7^{-/-}$WT mice, $\alpha7^{-/-}$iTat mice showed longer escape latency and longer cumulative distance on Day 3 (male mice) and on Day 4 (female mice), suggesting that Tat expression caused more severe learning impairment in $\alpha7^{-/-}$ mice. Furthermore, $\alpha7^{-/-}$WT mice had longer escape latency and longer cumulative distance than $\alpha7^{+/+}$WT on Day 4 (male mice), and only longer escape latency on Day 5 (female mice) and longer cumulative distance on all 5 days (female mice), indicating that α7 nAChR knockout itself also had negative effects on the learning of the mice, particularly on females. In the probe test, $\alpha7^{-/-}$iTat male mice had fewer platform entries, shorter time at target quadrant, time at the platform and distance to the platform than $\alpha7^{-/-}$WT male mice (Supplementary Fig. 2). $\alpha7^{-/-}$iTat male mice also showed shorter distance to target quadrant than $\alpha7^{+/+}$iTat male mice. In female mice, iTat mice showed longer latency to the platform and shorter time at target quadrant than wild-type mice. No other differences were noted among the different groups of mice.

Protein expression in cortex and hippocampus of these mice were also determined. In cortex, $\alpha7^{+/+}$iTat mice had higher PSD-95 than $\alpha7^{+/+}$WT mice, while no differences of PSD-95 were detected between $\alpha7^{-/-}$iTat mice and $\alpha7^{-/-}$WT mice (Fig. 2C, left and D, top left). $\alpha7^{-/-}$WT mice had lower GFAP than $\alpha7^{+/+}$WT mice, and $\alpha7^{-/-}$iTat mice had lower GFAP than $\alpha7^{+/+}$iTat mice and $\alpha7^{-/-}$WT mice. $\alpha7^{-/-}$iTat mice had higher Iba-1 than $\alpha7^{-/-}$WT mice and $\alpha7^{+/+}$iTat mice. In hippocampus, $\alpha7^{-/-}$iTat mice showed lower PSD-95

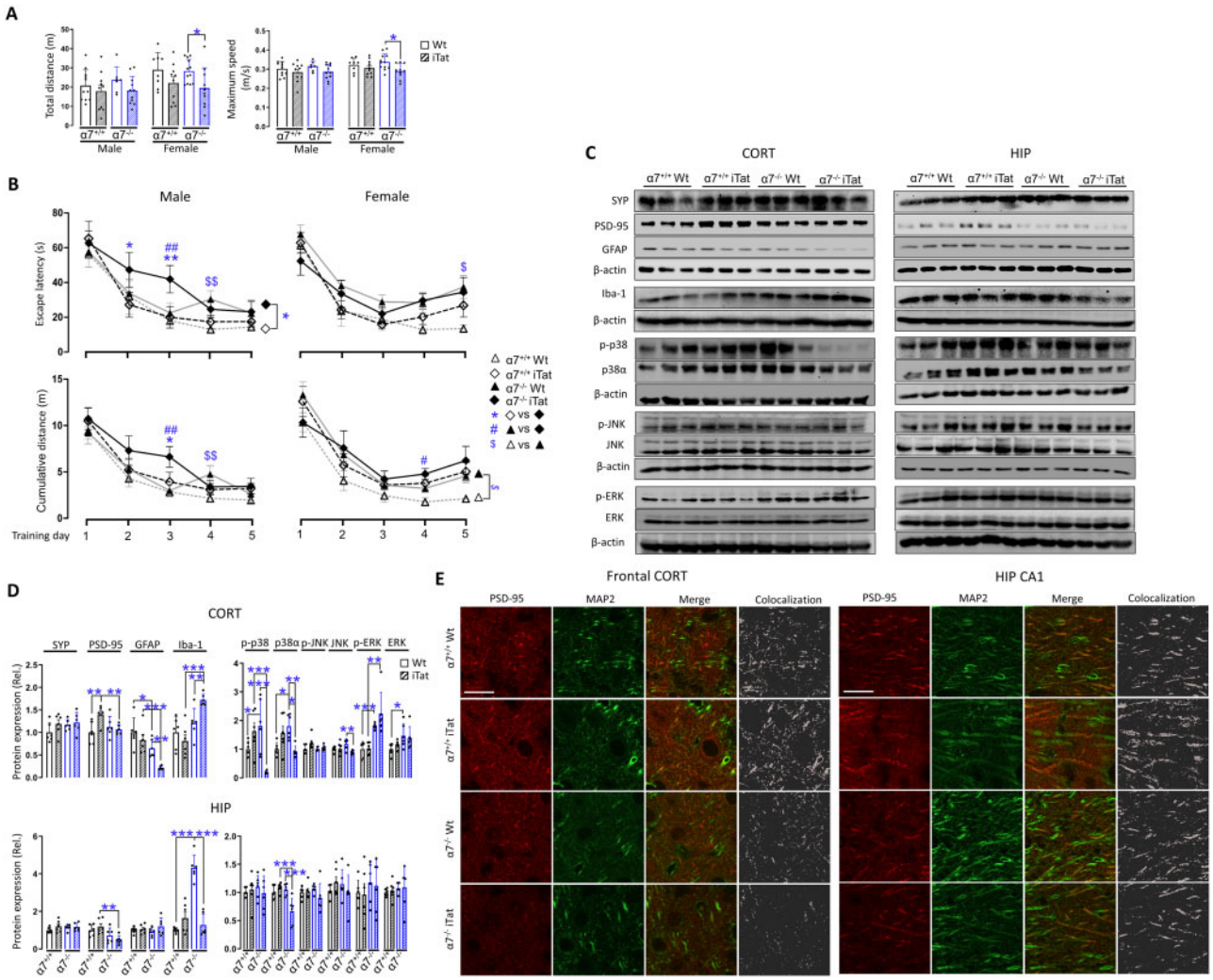

Figure 2 Effects of α7 nAChR knockout on PAM neuroprotection against Tat-induced behavioural impairments and neuropathologies. A similar experimental scheme was performed as in Fig. 1A except α7 nAChR knockout mice ($\alpha7^{-/-}$) and $\alpha7^{-/-}$iTat mice were used, which were obtained by cross-breeding $\alpha7^{-/-}$ mice with iTat mice and that the mice in all groups were receiving doxycycline-containing food pellets and PAM injections (n = 6–11/group). Similar behavioural open field test (**A**), Morris water maze training test (training stage, **B**), and western blotting (**C** and **D**) were performed (n = 6/group, three males and three females). Immunofluorescent staining was also performed for PSD-95 and MAP2 (**E**, scale bars = 20 μm). GT = genotype. $P < 0.05$ was considered significant and is indicated with asterisk, number symbol or dollar sign for comparisons among different groups; $^{**}P < 0.01$ and $^{***}P < 0.001$ were both considered highly significant and are indicated with asterisks. CORT = cortex; HIP = hippocampus.

than $\alpha7^{+/+}$iTat mice (Fig. 2C, right and D, bottom left). $\alpha7^{-/-}$WT mice had higher Iba-1 than $\alpha7^{+/+}$WT mice and $\alpha7^{-/-}$iTat mice. PSD-95 expression and its location were further confirmed by double immunofluorescent staining for PSD-95 and MAP2 (Fig. 2E). In regard to MAPK signalling pathways, in cortex, $\alpha7^{-/-}$iTat mice showed lower p38 and p-p38α than $\alpha7^{-/-}$WT and $\alpha7^{+/+}$iTat mice, while $\alpha7^{-/-}$WT mice showed higher p38 and p-p38α than $\alpha7^{+/+}$WT mice (Fig. 2C, left and D, top and right), further suggesting possible interplays among the α7 nAChR, HIV Tat neurotoxicity and p38 MAPK signalling pathway. In hippocampus, p38 and p-p38α showed similar trends but are lower only for p-p38α in $\alpha7^{-/-}$iTat mice (Fig. 2C, right and D, bottom and right). Only $\alpha7^{-/-}$iTat showed lower JNK than $\alpha7^{-/-}$WT in cortex. $\alpha7^{-/-}$WT had higher ERK and p-ERK than $\alpha7^{+/+}$WT in cortex, while $\alpha7^{-/-}$iTat had higher p-ERK than $\alpha7^{+/+}$iTat in cortex. No other differences were noted with JNK, p-JNK, ERK and p-ERK in hippocampus.

Taken together, we showed that α7 nAChR knockout abolished the neuroprotective effects of PAM against locomotor and learning and memory deficits of iTat mice. We also showed that α7 nAChR knockout specifically led to significant decreases of PSD-95 and p38α in both cortex and hippocampus, p-p38α in cortex and significant increases of Iba-1 in cortex of iTat mice. These findings confirm that α7 nAChR was directly involved in PAM neuroprotective function against Tat-induced behavioural impairments and neuropathologies.

p38 inhibition aggravated Tat-induced behavioural impairments and neuropathologies

The inverse correlation between Tat-induced behavioural impairments and neuropathologies and p38 expression and phosphorylation by PAM treatment (Fig. 1) and α7 nAChR knockout (Fig. 2) raised the possibility that p38 MAPK signalling pathway could be an important mediator of Tat neurotoxicity and PAM neuroprotective function against Tat neurotoxicity. To address this possibility, we took advantage of SB239063, a potent and selective p38 MAPK inhibitor and determined its effects on Tat-induced behavioural impairments and neuropathologies using the same experimental

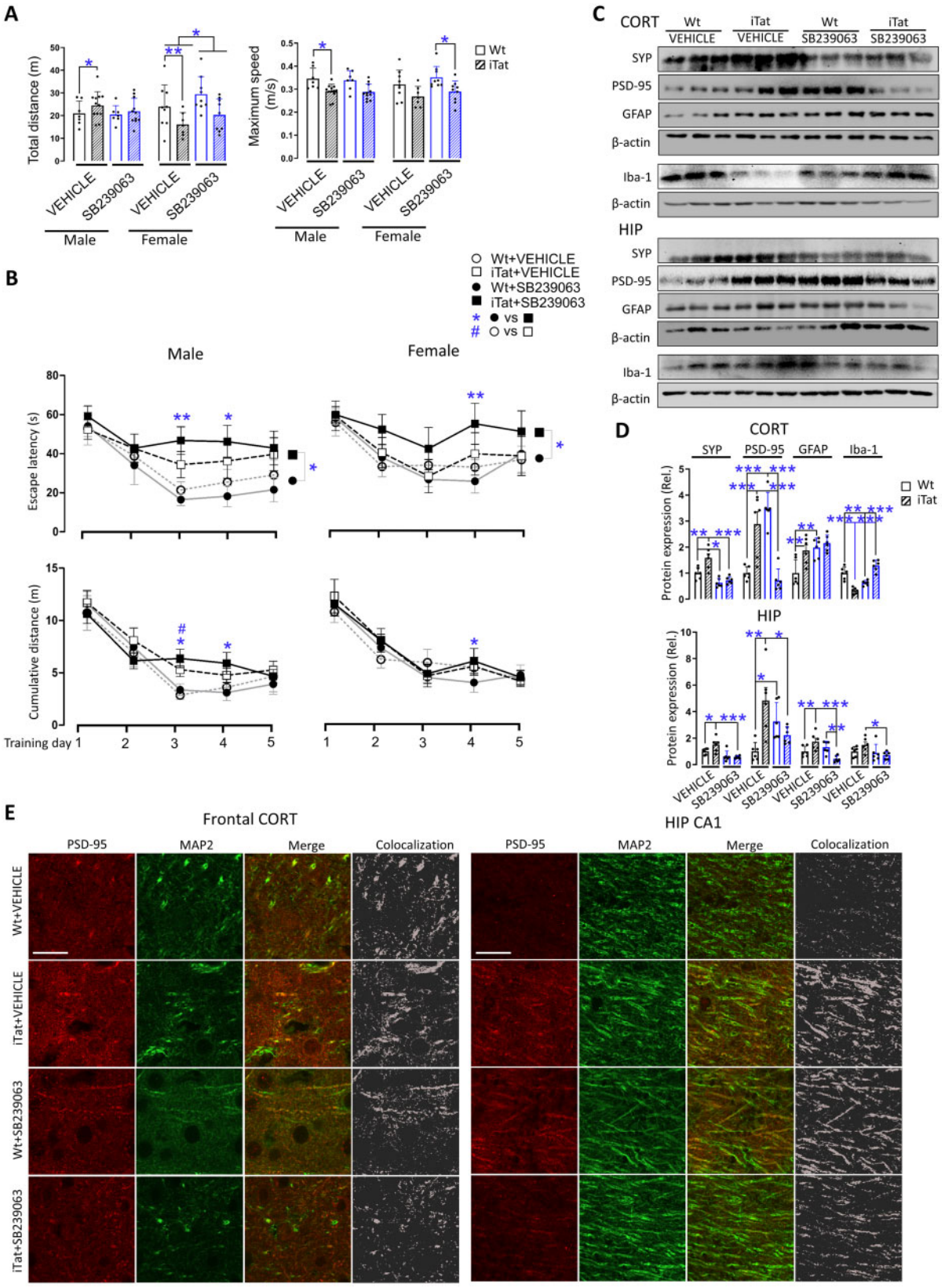

Figure 3 Effects of p38 MAPK inhibitor SB239063 on Tat-induced behavioural impairments and neuropathologies. A similar experimental scheme was performed as in Fig. 1A except for using intraperitoneal injection of p38 MAPK inhibitor SB239063 (15 mg/kg/day) in place of subcutaneous injection of PAM PNU-125096 for mice in all groups (n = 7–12/group). Similar behavioural open field test (**A**), Morris water maze test (training stage, **B**), western blotting (**C** and **D**, n = 6/group, only males; Results from females were shown in Supplementary Fig. 4), and immunofluorescent staining was performed for PSD-95 and MAP2 (**E**, scale bars = 20 μm). $P < 0.05$ was considered significant and is indicated with asterisk, number symbol or dollar sign for comparisons among different groups; $^{**}P < 0.01$ and $^{***}P < 0.001$ were both considered highly significant and are indicated with asterisks. CORT = cortex; HIP = hippocampus.

scheme as Fig. 1A, except for intraperitoneal injection of SB239063 in place of subcutaneous injection of PAM in these eight groups of mice (Table 1).

In the open field test, iTat mice showed a longer total travel distance than male wild-type mice and shorter travel distance than female wild-type mice, and slower maximum speed than male and female wild-type mice (Fig. 3A). SB239063 treatment led to no significant differences in travel distance and maximum speed between wild-type and iTat mice, both male and female. Notably, there was a difference of travel distance between SB239063-treated and vehicle-treated female mice, in both wild-type and iTat mice. In the Morris water maze training stage, male iTat mice showed a longer escape latency than male wild-type mice on all 5 days, while SB239063 treatment led to even longer escape latency than wild-type mice, with differences on Days 3 and 4 for male mice (Fig. 3B, top and left). Female iTat mice showed similar trends with difference on Day 4 compared with female wild-type mice (Fig. 3B, top and right). Similar patterns of the results were obtained about the cumulative distance, with the difference between vehicle-treated male iTat and male wild-type mice on Day 3 and difference between SB239063-treated male iTat and male wild-type mice on Days 2 and 3, and female iTat and wild-type mice on Day 4 (Fig. 3B, bottom). In the Morris water maze probe test, in the vehicle treatment, iTat male mice had shorter time at the target quadrant and distance to the target quadrant than wild-type male mice, while in the SB239063 treatment, male iTat mice had fewer platform entries, shorter distance to the target quadrant and distance to the platform than wild-type male mice (Supplementary Fig. 3). Except for the latency to the platform, in which SB239063-treated female iTat mice had longer latency than vehicle-treated female iTat mice, all SB239063-treated female iTat mice had fewer platform entries, shorter times at the target quadrant, distances to the target quadrant, time at the platform and distance to the platform than vehicle-treated female wild-type and iTat mice and SB239063-treated female wild-type mice.

Similarly, cortex and hippocampus of both male and female mice were analysed for protein expression, as they showed differential responses to the SB239063 treatment (Fig. 3C and D and Supplementary Fig. 4A and B). In cortex and hippocampus of both male and female mice, PSD-95 showed an identical pattern: vehicle-treated iTat mice had a higher PSD-95 than vehicle-treated wild-type mice, and SB239063-treated iTat mice had a lower PSD-95 than SB239063-treated wild-type mice (Fig. 3C and D and Supplementary Fig. 4A and B). All changes in PSD-95 were further verified by immunofluorescent staining, which also overlapped with MAP2 staining (Fig. 3E and Supplementary Fig. 4C). In both cortex and hippocampus of male mice, vehicle-treated iTat mice had higher SYP and GFAP than vehicle-treated wild-type mice, but SB239063-treated iTat mice showed no differences in SYN and GFAP (except hippocampus) from SB239063-treated wild-type mice (Fig. 3C and D). In both cortex and hippocampus of female mice, vehicle-treated iTat mice showed no differences of SYP, GFAP and Iba-1 from vehicle-treated wild-type mice, but SB239063-treated iTat mice showed lower SYP, GFAP and Iba-1 with differences from SB239063-treated wild-type mice (Supplementary Fig. 4A and B). There were other differences between individuals and groups, but with no consistent patterns.

Taken together, we showed that inhibition of p38 MAPK signalling pathway by SB239063 led to worsening learning and memory deficits in iTat mice and PSD-95 downregulation, and that SB239063 treatment showed no effects on the locomotor activity but showed sex-specific changes of protein expression of SYP and GFAP. These findings suggest strong interplays between p38 MAPK signalling pathway and PSD-95 in Tat neurotoxicity.

Differential response of neurons, microglia, astrocytes and neuron-astrocyte co-cultures to Tat and PAM

To ascertain our findings obtained from iTat mice and to elucidate relative roles of each type of brain cell in the interaction among the Tat neurotoxicity, PAM/α7 nAChR and p38 MAPK signalling pathway, we isolated primary cortical neurons, microglia and astrocytes from wild-type and α7 nAChR knockout mice, cultured them in the presence of Tat-containing conditioned medium (Tat-CM) or its control conditioned medium (Ctrl-CM) and in the presence of PAM and PNU-282987 (P2), or its solvent control DMSO for 24 h, and then determined expression levels of PSD-95, Iba-1, GFAP and p-p38 and p38 in these cells by western blotting. PNU-282987 (P2) was used as an α7 nAChR agonist in these *in vitro* experiments.

In the primary cortical neurons of wild-type mice, treatment of Tat, PAM+P2, or Tat plus PAM+P2, all showed lower PSD-95, p-p38 and p38 than the control treatment, while primary cortical neurons of $\alpha7^{-/-}$ mice showed similar effects, and treatments of these neurons with Tat, PAM+P2 or Tat plus PAM+P2 showed no further changes (Fig. 4A and B, top). In the microglia of wild-type mice, PAM+P2 or Tat plus PAM+P2 showed lower Iba-1, p-p38 and p38, while Tat alone increased Iba-1; In microglia of $\alpha7^{-/-}$ mice, only Tat (plus DMSO or PAM+P2) has higher Iba-1 than its control (plus DMSO or PAM+P2), and there were no differences in Iba-1 between DMSO and PAM+P2 (Fig. 4A and B, middle), which were consistent with our findings in cortex (Fig. 2C and D). Moreover, primary microglia of wild-type and $\alpha7^{-/-}$ mice under different treatments were visualized for their morphology (Fig. 4E), skeletonized (Fig. 4F) and calculated for the total length of the branches, indicative of microglia activation (Fig. 4G). In microglia of wild-type mice, Tat had shorter of branches than its control, while PAM+P2 had longer branches in both Tat and its control treatments. In microglia of $\alpha7^{-/-}$ mice, Tat had shorter branches than its control and there were no differences in the branch lengths between DMSO and PAM+P2. In astrocytes of wild-type mice, Tat had higher GFAP, p-p38 and p38, while Tat plus PAM+P2 had lower GFAP, but maintained the higher level of p-p38 and p38. In astrocytes of $\alpha7^{-/-}$ mice, only Tat (plus DMSO or PAM+P2) had lower GFAP and p-p38 than its control (plus DMSO or PAM+P2) and there were no differences of GFAP and p38 between DMSO and PAM+P2 (Fig. 4A and B, bottom), which were also consistent with our findings in cortex (Fig. 2C and D).

In addition, we also performed immunofluorescence staining of primary cortical neurons for PSD-95 (Fig. 4C) and quantified PSD-95 expression. Consistent with the findings from western blotting, Tat or PAM+P2 had lower PSD-95 than its control in wild-type neurons, and only Tat (DMSO and PAM+P2) had lower PSD-95 than its control (DMSO and PAM+P2) in $\alpha7^{-/-}$ neurons, and there were no differences of PSD-95 between DMSO and PAM+P2 (Fig. 4D).

To determine whether neuron-astrocyte interaction would be important for the interaction among the Tat neurotoxicity, PAM/α7 nAChR and p38 MAPK signalling pathway, similar experiments were performed using primary cortical neurons-astrocyte co-cultures from wild-type and α7 nAChR knockout mice. In the neuron-astrocyte co-cultures of wild-type mice, PAM+P2, Tat or Tat plus PAM+P2 all had higher PSD-95, p-p38 and p38, while in the neuron-astrocyte co-cultures of $\alpha7^{-/-}$ mice, only Tat (plus DMSO or PAM+P2) had a lower PSD-95, p-p38 and p38 than its control (plus DMSO or PAM+P2) and there were no differences in PSD-95, p-p38 and p38 between DMSO and PAM+P2 (Fig. 5A and B). Similar results were obtained for PSD-95 in neuron-astrocyte co-cultures (Fig. 5C and D). Taken together, we showed that Tat treatment led to significant lower PSD-95 in neurons and higher PSD-95 in neuron-

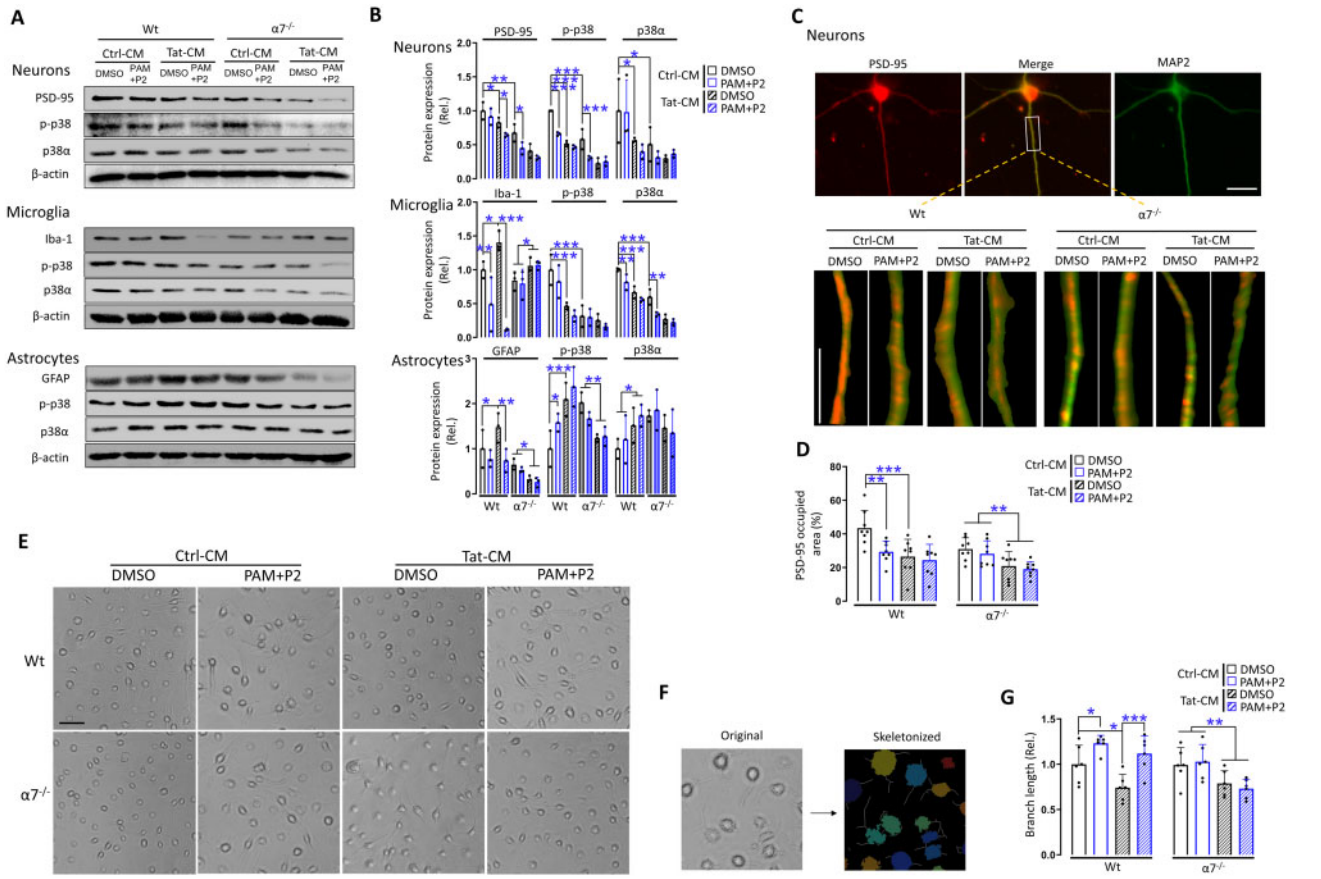

Figure 4 Response of primary neurons, microglia, astrocytes and neuron-astrocyte co-cultures to Tat and PAM. (**A**) Primary neurons, microglia, astrocytes were isolated from 1-day-old pups of wild-type (Wt) and $\alpha7^{-/-}$ mice, treated with the conditioned medium from pcDNA3-transfected cells (Ctrl-CM) or pcDNA3-Tat-transfected cells (Tat-CM) and PNU-125096 (PAM, 1 μM) and an α7 agonist PNU-282987 (P2, 0.5 μM) for 24 h and harvested to determine expression of PSD-95, Iba-1 or GFAP, or p-p38, p38 and β-actin by western blotting. (**B**) Protein expression was quantitated as in Fig. 1E. (**C**) Primary neurons were also double immunostained for PSD-95 and MAP2. (**D**) The positive staining area of PSD-95 puncta was quantitated by ImageJ. Primary microglia were visualized for their morphologies by microscopy before harvesting for cell lysates (**E**) and then skeletonized (**F**). The line shaped branches, indicative of the ramified stage, and their total length are quantified in **G**. The cells with shorter, non-completely formed or no line shaped branches were recognized as more amoeba-like phenotypes, which presented more often in only Tat treated wild-type group and α7- with Tat treatment groups (**A**). Multiple independent repeats were used for statistical analysis (n = 3/group for western blotting; n = 8/group for immunofluorescent staining, n = 6/group for microglia morphology). $P < 0.05$ was considered significant and is denoted with an asterisk; $^{**}P < 0.01$ and $^{***}P < 0.001$ were considered highly significant. Scale bars = 10 μm (**C**) and 50 μm (**E**).

astrocyte co-cultures, higher Iba-1 in microglia and higher GFAP in astrocytes, while PAM treatment led to lower PSD-95 in neurons, higher PSD-95 in neuron-astrocyte co-cultures, lower Iba-1 in microglia and lower GFAP in astrocytes, and α7 nAChR knockout plus Tat led to lower p-p38 and p38 with differences in neurons, microglia, astrocytes and neuron-astrocyte co-cultures. PSD-95 staining and microglia morphology showed similar results. These findings are consistent with the *in vivo* findings in mouse cortex (Figs 1E and F, 2D and E), and indicate that both microglia and astrocytes are important for the interaction among Tat neurotoxicity, PAM/α7 nAChR and p38 MAPK signalling pathway.

Microglia activation in mouse cortex in response to Tat, PAM and α7 nAChR knockout

To determine the relationship between microglia activation, Tat neurotoxicity and PAM/α7 nAChR, we performed the immunohistochemistry staining of microglia in cortex of wild-type and iTat mice treated with and without PAM (Fig. 1). Microglia were visualized for their morphology (Fig. 6A), and skeletonized (Fig. 6B) and quantitated for the number of branches and end points (Fig. 6C). iTat mice had more branches and end points than its wild-type control, PAM-treated iTat mice had fewer branches and end points than PAM-treated wild-type mice and DMSO-treated iTat mice. Similar immunohistochemistry staining was also performed with cortex of $\alpha7^{+/+}$WT, $\alpha7^{+/+}$iTat, $\alpha7^{-/-}$WT and $\alpha7^{-/-}$iTat mice in the presence of PAM (Fig. 2). $\alpha7^{-/-}$iTat mice had more branches and end points than $\alpha7^{-/-}$WT mice and $\alpha7^{-/-}$iTat mice (Fig. 6D and E). These findings further confirmed that microglia activation was directly involved in Tat neurotoxicity and its interaction with PAM/α7 nAChR.

Discussion

In this study, we first showed that PAM treatment greatly improved locomotor activity, learning and memory of iTat mice, and increased PSD-95 expression and decreased GFAP and Iba-1 expression in cortex of iTat mice. We next showed that knockout of α7 nAChR abolished PAM protection against Tat-induced neurotoxicity. α7 nAChR expression was detected in both cortex and hippocampus of iTat mice, although its expression was increased in cortex by either Tat expression or PAM treatment but only decreased in hippocampus by both Tat expression and PAM treatment (Supplementary Fig. 5A–C). In addition, PAM/P2 treatment

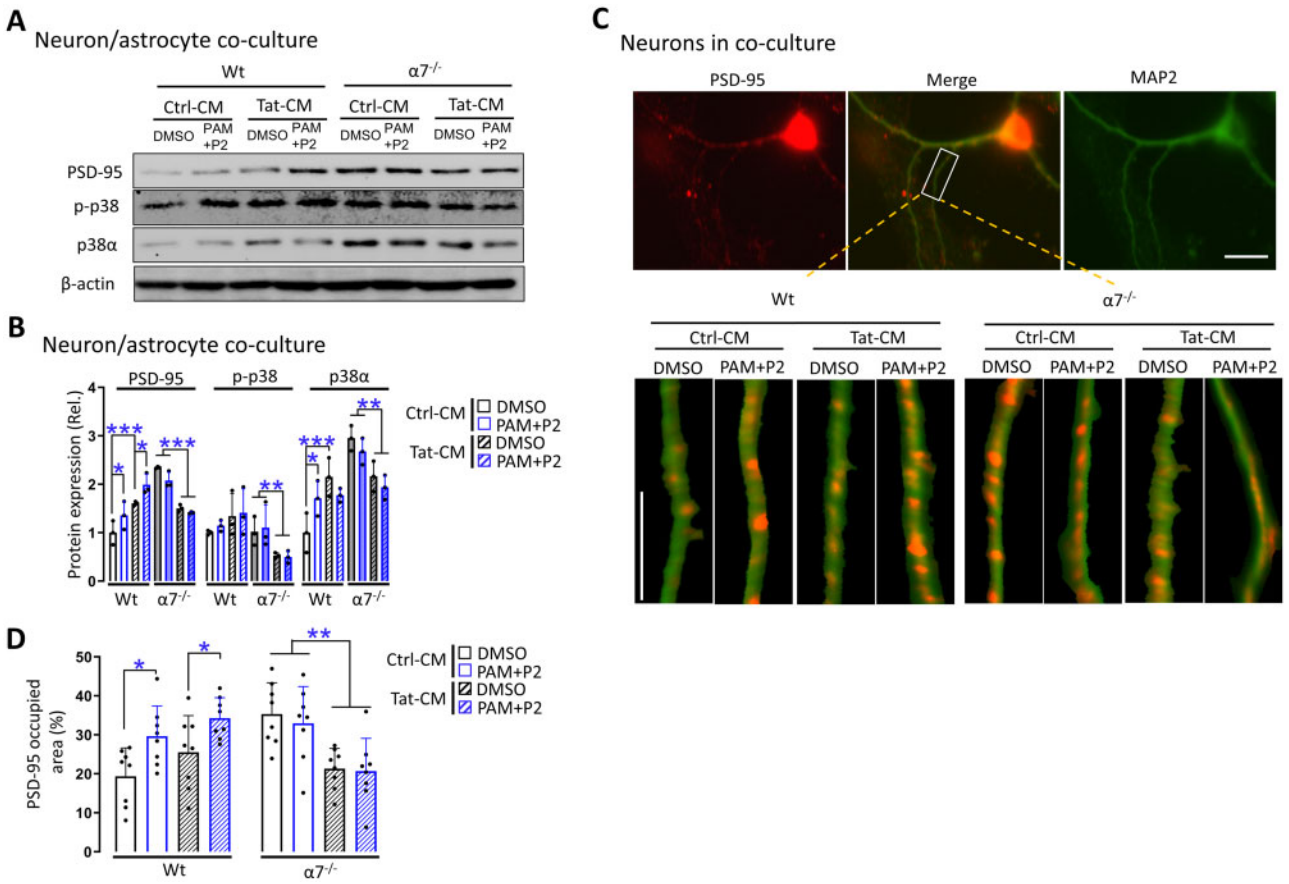

Figure 5 Response of neuron-astrocyte co-cultures to Tat and PAM. (**A**) Primary cortical neurons-astrocytes were isolated from 1-day-old pups of wild-type (Wt) and $\alpha7^{-/-}$ mice, treated with the conditioned medium from pcDNA3-transfected cells (Ctrl-CM) or pcDNA3-Tat-transfected cells (Tat-CM) and PNU-125096 (PAM, 1 μM) and an α7 agonist PNU-282987 (P2, 0.5 μM) for 24 h, and harvested to determine expression of PSD-95, p-p38 and p38 and β-actin by western blotting. (**B**) Protein expression was quantitated. Primary neurons were also double immunostained for PSD-95 (red) and MAP2 (green) (**C**) and quantitated for PSD-95 (**D**). Multiple independent repeats were used for statistical analysis ($n = 3$/group for western blotting). $P < 0.05$ was considered significant and is denoted with an asterisk; $^{**}P < 0.01$ and $^{***}P < 0.001$ were considered highly significant. Scale bars = 10 μm (**C**).

led to decreased α7 nAChR expression in neurons but increased α7 nAChR expression in microglia and astrocytes, while Tat led to increased α7 nAChR expression in microglia and astrocytes but decreased α7 nAChR expression in neurons (Supplementary Fig. 5D and E). These results demonstrated that α7 nAChR expression was directly involved in PAM neuroprotective activity against Tat neurotoxicity, but changes of α7 nAChR expression in response to Tat and PAM treatment was brain region- and cell type-dependent. Thus, the changes of α7 nAChR expression in response to Tat and PAM treatment alone could not account for the PAM neuroprotective effects in this study. Furthermore, it is quite reasonable to assume that α7 nAChR is expressed in the brain of other rodent HAND models, even though no studies about α7 nAChR expression in these models are currently available.

In addition, we showed that inhibition of p38 MAPK signalling pathway worsened Tat-induced learning and memory impairments and was associated with downregulation of PSD-95 in both cortex and hippocampus. Inhibition of p38 MAPK signalling pathway has led to improved cognition, learning and memory in several neurological diseases.[78–83] We indeed noted some beneficial effects in the wild-type mice when treated with p38 MAPK inhibitor SB239063. On the other hand, PSD-95 up-regulation and improved behaviours were noted with PAM-treated iTat mice while little p38 MAPK was altered in iTat mice in the absence of PAM treatment. These results together indicate p38 MAPK regulation of PSD-95 expression is involved in PAM-activated α7 nAChR-mediated protection against Tat neurotoxicity and that p38 MAPK activation is not involved in Tat neurotoxicity, at least at the level of Tat expression in the brain of these iTat mice. *In vitro* studies on the involvement of p38 MAPK on Tat neurotoxicity are not consistent. For instance, inhibition of p38 by SB203580 failed to block Tat-induced neurite losses and cell death in striatal neurons,[84] but prevented Tat-induced apoptosis in cerebellar granule neurons.[85] Moreover, inhibition of p38 MAPK by a different inhibitor SB202190 decreased Tat-induced inflammation and oxidation in hippocampal slice cultures.[46] Several factors could contribute to these inconsistencies. First, the specificity of the inhibitors differs. SB203580 and SB202190 both have shown off-target effects.[86] SB239063, the inhibitor used in this study is the second generation of p38 MAPK inhibitor and is much more selective and more popular for neurological disease studies;[82] Second, *in vitro* experimental systems differ. For example, different types of neuron cultures were used. Last and more plausibly, higher concentrations of Tat were often used in these *in vitro* experiments than that in the brain of the iTat mice, while Tat expression in the brain of iTat mice[87] is more relevant to that in the HIV-infected brain in the era of antiretroviral therapy.[26,27] Interestingly, we also noted that both female wild-type and female iTat mice performed better in the open field test than male wild-type and male iTat mice in response to SB239063, which was consistent with higher SYP in cortex of the

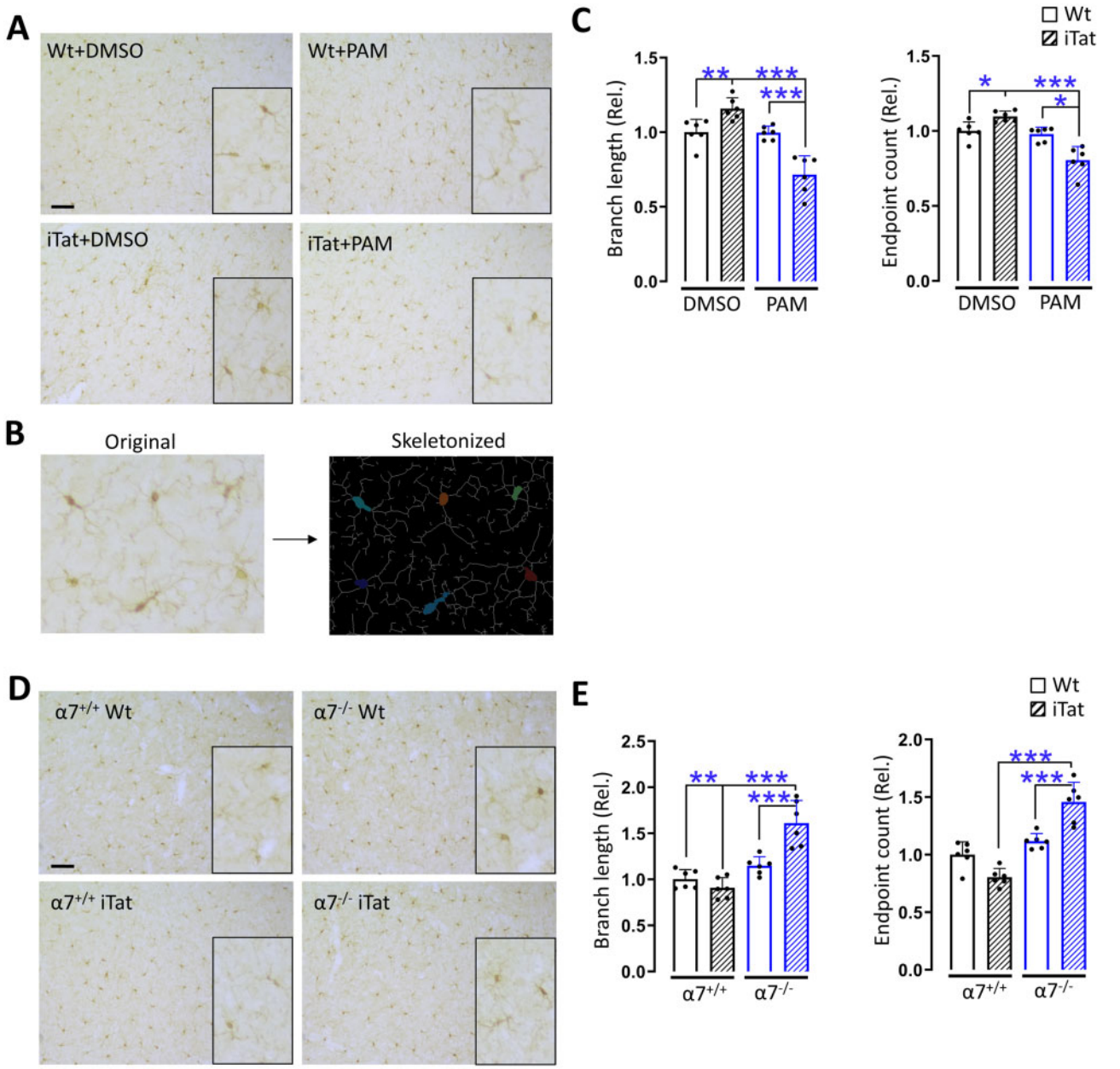

Figure 6 Microglia activation by PAM in cortex of iTat mice and $\alpha7^{-/-}$ iTat mice. (**A**) The brains from Fig. 1 were dissected, fixed, sectioned and stained for Iba-1. Microglia morphologies were skeletonized (**B**), and the total length and end points of branches in three brain regions including prefrontal, parietal and occipital cortex were quantified and averaged from three sections of each mouse ($n = 6$/group, 3 males and 3 females) (**C**). Similarly, the brains from Fig. 2 were processed and stained for Iba-1 (**D**), skeletonized and quantitated (**E**). The WT+DMSO group was used as a reference and set at 1. $P < 0.05$ was considered significant and is denoted with an asterisk; $^{**}P < 0.01$ and $^{***}P < 0.001$ were considered highly significant. Scale bars = 200 μm (**A**).

female mice than male mice. These results suggest the unique roles of p38 MAPK signalling pathway in sex-dependent specific behavioural changes of iTat mice and that SYP expression in cortex is associated with locomotor activity control.

We also determined neuropathological changes in response to PAM treatment and α7 nAChR knockout, by focusing on neuronal markers SYP and PSD-95, and microglia marker Iba-1 and astrocyte marker GFAP in two important brain regions, cortex and hippocampus. SYP showed no significance changes in both cortex and hippocampus of iTat mice when treated with PAM in the presence and absence of α7 nAChR, which was further confirmed by immunofluorescent staining (Supplementary Fig. 6). PSD-95 showed increases in both cortex and hippocampus of wild-type and iTat mice and PAM treatment led to more increases, while α7 nAChR led to decreases of PSD-95 in both cortex and hippocampus of iTat mice in the presence of PAM. Similar results were obtained in our subsequent neuron-astrocyte co-cultures with and without α7 nAChR expression. Nevertheless, we and others have shown that Tat induces PSD-95 down-regulation when Tat-expressing conditioned medium from astrocytes was used to treat neurons or using recombinant Tat protein in a trans-well setting of astrocytes and neurons without direct contact.[37,88] These studies further support the hypothesis that astrocytes are the key regulator of Tat neurotoxicity and suggest that the cell–cell interaction between astrocytes and neurons is important for this regulatory role.

Besides SYP and PSD-95, we also showed significant changes of Iba-1 and GFAP in response to the Tat, PAM/α7 nAChR and p38 MAPK signalling pathway. Tat expression led to increases of GFAP expression and PAM treatment completely reversed the increases in cortex and *in vitro*. A similar response was obtained with Iba-1. α7 nAChR knockout further abrogated PAM effects on Tat-induced Iba-1 expression but not GFAP expression, suggesting distinct roles of α7 nAChR in astrocytes. α7 nAChR expressed in these non-excitable glia cells is usually associated with its anti-inflammatory role.[89] However, we failed to detect infiltrates of immune cells in Tat-expressing brain of the iTat mice (Supplementary Fig. 7). We also failed to detect significant changes of pro-inflammatory cytokines/chemokines such as TNF-α in the brain of iTat mice and in *in vitro* Tat-containing conditioned medium-treated primary microglia and astrocytes (Supplementary Fig. 8), despite the fact that astrogliosis and microgliosis were clearly detected by the current study and our previous studies.[32,38] Taken together, the results demonstrated that activation of microglia and astrocytes were important links among Tat neurotoxicity, PAM/α7 nAChR interaction and p38 MAPK signalling pathway and suggest that α7 nAChR anti-inflammatory property is not primarily responsible for PAM neuroprotective effects against Tat neurotoxicity. Of note were differences of GFAP and Iba-1 expression in cortex and hippocampus and their differential responses to PAM/α7 nAChR activation, which may result from the cell heterogeneity in different brain regions and different expression of α7 nAChR in these cells.

Importantly, the findings from the current study raised the possibility that PSD-95 is the convergent link involved in the interplays between Tat neurotoxicity and α7 nAChR activation. PSD95 participates in synapse formation, maturation and plasticity and glutamate-mediated neurotoxicity,[90] its loss leads to abnormal LTP, impairs learning and memory process,[91–93] and is involved in several neurological and psychiatric diseases.[94–97] Tat binds to LRP[23] and induces LRP/PSD-95/NMDAR complex formation potentiates glutamate excitotoxicity and promotes neuronal apoptosis.[98] Therapeutic approaches have been proposed to disrupt PSD-95/NMDAR complex to ameliorate pathological changes.[99–101] Meanwhile, our results showed increased PSD-95 expression was closely associated with improved learning and memory and locomotor activity. It is possible that increased PSD-95 serves as a compensatory mechanism for its loss in formation of abnormal complexes and to enhance its synaptic function, as evidenced in studies in which increased PSD-95 correlates with its protective effects in Alzheimer's disease and Parkinson's disease animal models.[102–104]

In conclusion, we showed that PAM treatment led to significant protection against Tat-induced locomotor, learning and memory impairments and astrocyte/microglia activation and neuronal injury. We also showed that α7 nAChR activation, followed by p38 MAPK-mediated PSD-95 expression contributed to PAM-induced neuroprotection against Tat neurotoxicity. These findings demonstrate for the first time that α7 nAChR and its PAM hold significant therapeutic promise for development of therapeutics for HAND.

Funding

This work was supported in part by grants R01DA043162 and R01NS094108 (J.J.H.) from US National Institutes of Health.

Competing interests

The authors report no competing interests.

Supplementary material

Supplementary material is available at *Brain* online.

References

1. Munoz A, Sabin CA, Phillips AN. The incubation period of AIDS. *AIDS*. 1997;11 (Suppl A):S69–S76.
2. Survival after introduction of HAART in people with known duration of HIV-1 infection. The CASCADE Collaboration. Concerted Action on SeroConversion to AIDS and Death in Europe. *Lancet*. 2000;355:1158–1159.
3. Egger M, May M, Chêne G, et al.; ART Cohort Collaboration. Prognosis of HIV-1-infected patients starting highly active antiretroviral therapy: A collaborative analysis of prospective studies. *Lancet*. 2002;360(9327):119–129.
4. May M, Sterne JAC, Sabin C, et al.; Antiretroviral Therapy (ART) Cohort Collaboration. Prognosis of HIV-1-infected patients up to 5 years after initiation of HAART: Collaborative analysis of prospective studies. *AIDS*. 2007;21(9):1185–1197.
5. May MT, Sterne JAC, Costagliola D, et al.; Antiretroviral Therapy (ART) Cohort Collaboration. HIV treatment response and prognosis in Europe and North America in the first decade of highly active antiretroviral therapy: A collaborative analysis. *Lancet*. 2006;368(9534):451–458.
6. Cysique LA, Maruff P, Brew BJ. Prevalence and pattern of neuropsychological impairment in human immunodeficiency virus-infected/acquired immunodeficiency syndrome (HIV/AIDS) patients across pre- and post-highly active antiretroviral therapy eras: A combined study of two cohorts. *J Neurovirol*. 2004;10(6):350–357.
7. Masliah E, DeTeresa RM, Mallory ME, Hansen LA. Changes in pathological findings at autopsy in AIDS cases for the last 15 years. *AIDS*. 2000;14(1):69–74.
8. Ellis R, Langford D, Masliah E. HIV and antiretroviral therapy in the brain: Neuronal injury and repair. *Nat Rev Neurosci*. 2007;8(1):33–44.
9. d'Arminio Monforte A, Cinque P, Mocroft A, et al.; EuroSIDA Study Group. Changing incidence of central nervous system diseases in the EuroSIDA cohort. *Ann Neurol*. 2004;55(3):320–328.
10. Sacktor N, Lyles RH, Skolasky R, et al.; Multicenter AIDS Cohort Study. HIV-associated neurologic disease incidence changes: Multicenter AIDS Cohort Study, 1990-1998. *Neurology*. 2001;56(2):257–260.
11. Sacktor N, McDermott MP, Marder K, et al. HIV-associated cognitive impairment before and after the advent of combination therapy. *J Neurovirol*. 2002;8(2):136–142.
12. Giancola ML, Lorenzini P, Balestra P, et al. Neuroactive antiretroviral drugs do not influence neurocognitive performance in less advanced HIV-infected patients responding to highly active antiretroviral therapy. *J Acquir Immune Defic Syndr*. 2006;41(3):332–337.
13. Dawes S, Suarez P, Casey CY, et al.; HNRC Group. Variable patterns of neuropsychological performance in HIV-1 infection. *J Clin Exp Neuropsychol*. 2008;30(6):613–626.
14. Langford TD, Letendre SL, Larrea GJ, Masliah E. Changing patterns in the neuropathogenesis of HIV during the HAART era. *Brain Pathol*. 2003;13(2):195–210.
15. Heaton RK, Marcotte TD, Mindt MR, et al.; HNRC Group. The impact of HIV-associated neuropsychological impairment on everyday functioning. *J Int Neuropsychol Soc*. 2004;10(3):317–331.
16. Letendre S, Marquie-Beck J, Capparelli E, et al.; CHARTER Group. Validation of the CNS penetration-effectiveness rank for quantifying antiretroviral penetration into the central nervous system. *Arch Neurol*. 2008;65(1):65–70.
17. Yilmaz A, Price RW, Gisslen M. Antiretroviral drug treatment of CNS HIV-1 infection. *J Antimicrob Chemother*. 2012;67(2):299–311.

18. Caniglia EC, Cain LE, Justice A, et al.; On behalf of the HIV-CAUSAL Collaboration. Antiretroviral penetration into the CNS and incidence of AIDS-defining neurologic conditions. *Neurology*. 2014;83(2):134–141.
19. Heaton RK, Clifford DB, Franklin DR, et al. CHARTER Group. HIV-associated neurocognitive disorders persist in the era of potent antiretroviral therapy: CHARTER Study. *Neurology*. 2010; 75(23):2087–2096.
20. Bagasra O, Lavi E, Bobroski L, et al. Cellular reservoirs of HIV-1 in the central nervous system of infected individuals: Identification by the combination of in situ polymerase chain reaction and immunohistochemistry. *AIDS*. 1996;10(6):573–585.
21. Wallet C, De Rovere M, Van Assche J, et al. Microglial cells: The main HIV-1 reservoir in the brain. *Front Cell Infect Microbiol*. 2019;9:362.
22. Brack-Werner R. Astrocytes: HIV cellular reservoirs and important participants in neuropathogenesis. *AIDS*. 1999;13(1):1–22.
23. Liu Y, Jones M, Hingtgen CM, et al. Uptake of HIV-1 Tat protein mediated by low-density lipoprotein receptor-related protein disrupts the neuronal metabolic balance of the receptor ligands. *Nat Med*. 2000;6(12):1380–1387.
24. Frankel AD, Pabo CO. Cellular uptake of the Tat protein from human immunodeficiency virus. *Cell*. 1988;55(6):1189–1193.
25. Hudson L, Liu J, Nath A, et al. Detection of the human immunodeficiency virus regulatory protein Tat in CNS tissues. *J Neurovirol*. 2000;6(2):145–155.
26. Johnson TP, Patel K, Johnson KR, et al. Induction of IL-17 and nonclassical T-cell activation by HIV-Tat protein. *Proc Natl Acad Sci U S A*. 2013;110(33):13588–13593.
27. Henderson LJ, Johnson TP, Smith BR, et al. Presence of Tat and transactivation response element in spinal fluid despite antiretroviral therapy. *AIDS*. 2019;33 (Suppl 2):S145–S157.
28. Zhou BY, Liu Y, Kim B, Xiao Y, He JJ. Astrocyte activation and dysfunction and neuron death by HIV-1 Tat expression in astrocytes. *Mol Cell Neurosci*. 2004;27(3):296–305.
29. Zhou BY, He JJ. Proliferation inhibition of astrocytes, neurons, and non-glial cells by intracellularly expressed human immunodeficiency virus type 1 (HIV-1) Tat protein. *Neurosci Lett*. 2004;359(3):155–158.
30. Zou W, Kim BO, Zhou BY, et al. Protection against human immunodeficiency virus type 1 Tat neurotoxicity by ginkgo biloba extract EGb 761 involving glial fibrillary acidic protein. *Am J Pathol*. 2007;171(6):1923–1935.
31. Fan Y, Zou W, Green LA, Kim BO, He JJ. Activation of Egr-1 expression in astrocytes by HIV-1 Tat: New insights into astrocyte-mediated Tat neurotoxicity. *J Neuroimmune Pharmacol*. 2011;6(1):121–129.
32. Zou W, Wang Z, Liu Y, et al. Involvement of p300 in constitutive and HIV-1 Tat-activated expression of glial fibrillary acidic protein in astrocytes. *Glia*. 2010;58(13):1640–1648.
33. Fields J, Dumaop W, Eleuteri S, et al. HIV-1 Tat alters neuronal autophagy by modulating autophagosome fusion to the lysosome: Implications for HIV-associated neurocognitive disorders. *J Neurosci*. 2015;35(5):1921–1938.
34. Fan Y, Gao X, Chen J, Liu Y, He JJ. HIV Tat impairs neurogenesis through functioning as a notch ligand and activation of notch signaling pathway. *J Neurosci*. 2016;36(44):11362–11373.
35. Fan Y, He JJ. HIV-1 Tat promotes lysosomal exocytosis in astrocytes and contributes to astrocyte-mediated tat neurotoxicity. *J Biol Chem*. 2016;291(43):22830–22840.
36. Fan Y, He JJ. HIV-1 Tat induces unfolded protein response and endoplasmic reticulum stress in astrocytes and causes neurotoxicity through glial fibrillary acidic protein (GFAP) activation and aggregation. *J Biol Chem*. 2016;291(43): 22819–22829.
37. Rahimian P, He JJ. HIV-1 Tat-shortened neurite outgrowth through regulation of microRNA-132 and its target gene expression. *J Neuroinflammation*. 2016;13(1):247.
38. Kim BO, Liu Y, Ruan Y, et al. Neuropathologies in transgenic mice expressing human immunodeficiency virus type 1 Tat protein under the regulation of the astrocyte-specific glial fibrillary acidic protein promoter and doxycycline. *Am J Pathol*. 2003;162(5):1693–1707.
39. Raybuck JD, Hargus NJ, Thayer SA. A GluN2B-selective NMDAR antagonist reverses synapse loss and cognitive impairment produced by the HIV-1 protein Tat. *J Neurosci*. 2017;37(33):7837–7847.
40. Kesby JP, Markou A, Semenova S. The effects of HIV-1 regulatory TAT protein expression on brain reward function, response to psychostimulants and delay-dependent memory in mice. *Neuropharmacology*. 2016;109:205–215.
41. Nookala AR, Schwartz DC, Chaudhari NS, et al. Methamphetamine augment HIV-1 Tat mediated memory deficits by altering the expression of synaptic proteins and neurotrophic factors. *Brain Behav Immun*. 2018;71:37–51.
42. Carey AN, Sypek EI, Singh HD, Kaufman MJ, McLaughlin JP. Expression of HIV-Tat protein is associated with learning and memory deficits in the mouse. *Behav Brain Res*. 2012;229(1): 48–56.
43. Li S-T, Matsushita M, Moriwaki A, et al. HIV-1 Tat inhibits long-term potentiation and attenuates spatial learning [corrected]. *Ann Neurol*. 2004;55(3):362–371.
44. Moran LM, Fitting S, Booze RM, Webb KM, Mactutus CF. Neonatal intrahippocampal HIV-1 protein Tat(1-86) injection: Neurobehavioral alterations in the absence of increased inflammatory cytokine activation. *Int J Dev Neurosci*. 2014;38: 195–203.
45. Hahn YK, Podhaizer EM, Farris SP, et al. Effects of chronic HIV-1 Tat exposure in the CNS: Heightened vulnerability of males versus females to changes in cell numbers, synaptic integrity, and behavior. *Brain Struct Funct*. 2015;220(2):605–623.
46. Fu X, Lawson MA, Kelley KW, Dantzer R. HIV-1 Tat activates indoleamine 2,3 dioxygenase in murine organotypic hippocampal slice cultures in a p38 mitogen-activated protein kinase-dependent manner. *J Neuroinflammation*. 2011;8:88.
47. Gotti C, Zoli M, Clementi F. Brain nicotinic acetylcholine receptors: Native subtypes and their relevance. *Trends Pharmacol Sci*. 2006;27(9):482–491.
48. Albuquerque EX, Pereira EF, Alkondon M, Rogers SW. Mammalian nicotinic acetylcholine receptors: From structure to function. *Physiol Rev*. 2009;89(1):73–120.
49. Hoskin JL, Al-Hasan Y, Sabbagh MN. Nicotinic acetylcholine receptor agonists for the treatment of Alzheimer's Dementia: an update. *Nicotine Tob Res*. 2019;21(3):370–376.
50. Bouzat C, Lasala M, Nielsen BE, Corradi J, Esandi MDC. Molecular function of alpha7 nicotinic receptors as drug targets. *J Physiol*. 2018;596(10):1847–1861.
51. King JR, Nordman JC, Bridges SP, Lin MK, Kabbani N. Identification and characterization of a G protein-binding cluster in alpha7 nicotinic acetylcholine receptors. *J Biol Chem*. 2015;290(33):20060–20070.
52. Dajas-Bailador FA, Soliakov L, Wonnacott S. Nicotine activates the extracellular signal-regulated kinase 1/2 via the alpha7 nicotinic acetylcholine receptor and protein kinase A, in SH-SY5Y cells and hippocampal neurones. *J Neurochem*. 2002;80(3): 520–530.
53. Dineley KT, Westerman M, Bui D, et al. Beta-amyloid activates the mitogen-activated protein kinase cascade via hippocampal alpha7 nicotinic acetylcholine receptors: In vitro and in vivo mechanisms related to Alzheimer's disease. *J Neurosci*. 2001;21(12):4125–4133.

54. El Kouhen R, Hu M, Anderson DJ, Li J, Gopalakrishnan M. Pharmacology of alpha7 nicotinic acetylcholine receptor mediated extracellular signal-regulated kinase signalling in PC12 cells. *Br J Pharmacol*. 2009;156(4):638–648.
55. King JR, Kabbani N. Alpha 7 nicotinic receptor coupling to heterotrimeric G proteins modulates RhoA activation, cytoskeletal motility, and structural growth. *J Neurochem*. 2016;138(4):532–545.
56. Egea J, Buendia I, Parada E, et al. Anti-inflammatory role of microglial alpha7 nAChRs and its role in neuroprotection. *Biochem Pharmacol*. 2015;97(4):463–472.
57. Kim H, Kim SR, Je J, et al. The proximal tubular alpha7 nicotinic acetylcholine receptor attenuates ischemic acute kidney injury through Akt/PKC signaling-mediated HO-1 induction. *Exp Mol Med*. 2018;50(4):1–17.
58. Larsen HM, Hansen SK, Mikkelsen JD, Hyttel P, Stummann TC. Alpha7 nicotinic acetylcholine receptors and neural network synaptic transmission in human induced pluripotent stem cell-derived neurons. *Stem Cell Res*. 2019;41:101642.
59. Buckingham SD, Jones AK, Brown LA, Sattelle DB. Nicotinic acetylcholine receptor signalling: Roles in Alzheimer's disease and amyloid neuroprotection. *Pharmacol Rev*. 2009;61(1):39–61.
60. Xu S, Yang B, Tao T, et al. Activation of alpha7-nAChRs protects SH-SY5Y cells from 1-methyl-4-phenylpyridinium-induced apoptotic cell death via ERK/p53 signaling pathway. *J Cell Physiol*. 2019;234(10):18480–18491.
61. Tregellas JR, Wylie KP. Alpha7 nicotinic receptors as therapeutic targets in schizophrenia. *Nicotine Tob Res*. 2019;21(3):349–356.
62. Rahman S, Engleman EA, Bell RL. Nicotinic receptor modulation to treat alcohol and drug dependence. *Front Neurosci*. 2014;8:426.
63. Xiao C, Zhou CY, Jiang JH, Yin C. Neural circuits and nicotinic acetylcholine receptors mediate the cholinergic regulation of midbrain dopaminergic neurons and nicotine dependence. *Acta Pharmacol Sin*. 2020;41(1):1–9.
64. Mineur YS, Mose TN, Blakeman S, Picciotto MR. Hippocampal alpha7 nicotinic ACh receptors contribute to modulation of depression-like behaviour in C57BL/6J mice. *Br J Pharmacol*. 2018;175(11):1903–1914.
65. Liu Q, Liu C, Jiang L, et al. Alpha7 Nicotinic acetylcholine receptor-mediated anti-inflammatory effect in a chronic migraine rat model via the attenuation of glial cell activation. *J Pain Res*. 2018;11:1129–1140.
66. Koukouli F, Rooy M, Tziotis D, et al. Nicotine reverses hypofrontality in animal models of addiction and schizophrenia. *Nat Med*. 2017;23(3):347–354.
67. Jones CK, Byun N, Bubser M. Muscarinic and nicotinic acetylcholine receptor agonists and allosteric modulators for the treatment of schizophrenia. *Neuropsychopharmacology*. 2012;37(1):16–42.
68. Sun F, Johnson SR, Jin K, Uteshev VV. Boosting endogenous resistance of brain to ischemia. *Mol Neurobiol*. 2017;54(3):2045–2059.
69. Dash PK, Zhao J, Kobori N, et al. Activation of alpha 7 cholinergic nicotinic receptors reduce blood-brain barrier permeability following experimental traumatic brain injury. *J Neurosci*. 2016;36(9):2809–2818.
70. Capo-Velez CM, et al. The alpha7-nicotinic receptor contributes to gp120-induced neurotoxicity: Implications in HIV-associated neurocognitive disorders. *Sci Rep*. 2018;8:1829.
71. Liu L, Yu J, Li L, et al. Alpha7 nicotinic acetylcholine receptor is required for amyloid pathology in brain endothelial cells induced by Glycoprotein 120, methamphetamine and nicotine. *Sci Rep*. 2017;7:40467.
72. Zhang B, Yu J-Y, Liu L-Q, et al. Alpha7 nicotinic acetylcholine receptor is required for blood-brain barrier injury-related CNS disorders caused by *Cryptococcus neoformans* and HIV-1 associated comorbidity factors. *BMC Infect Dis*. 2015;15:352.
73. Uteshev VV. Allosteric modulation of nicotinic acetylcholine receptors: The concept and therapeutic trends. *Curr Pharm Des*. 1986;22:1997–2016.
74. Uteshev VV. The therapeutic promise of positive allosteric modulation of nicotinic receptors. *Eur J Pharmacol*. 2014;727:181–185.
75. Yang JS, Seo SW, Jang S, Jung GY, Kim S. Rational engineering of enzyme allosteric regulation through sequence evolution analysis. *PLoS Comput Biol*. 2012;8(7):e1002612.
76. McLean SL, Idris NF, Grayson B, et al. PNU-120596, a positive allosteric modulator of alpha7 nicotinic acetylcholine receptors, reverses a sub-chronic phencyclidine-induced cognitive deficit in the attentional set-shifting task in female rats. *J Psychopharmacol*. 2012;26(9):1265–1270.
77. Gibbs KL, Kalmar B, Rhymes ER, et al. Inhibiting p38 MAPK alpha rescues axonal retrograde transport defects in a mouse model of ALS. *Cell Death Dis*. 2018;9(6):596.
78. Mannangatti P, NarasimhaNaidu K, Damaj MI, Ramamoorthy S, Jayanthi LD. A role for p38 mitogen-activated protein kinase-mediated threonine 30-dependent norepinephrine transporter regulation in cocaine sensitization and conditioned place preference. *J Biol Chem*. 2015;290(17):10814–10827.
79. Maphis N, Jiang S, Xu G, et al. Selective suppression of the alpha isoform of p38 MAPK rescues late-stage tau pathology. *Alzheimers Res Ther*. 2016;8(1):54.
80. Robson MJ, Quinlan MA, Margolis KG, et al. p38alpha MAPK signaling drives pharmacologically reversible brain and gastrointestinal phenotypes in the SERT Ala56 mouse. *Proc Natl Acad Sci U S A*. 2018;115(43):E10245–E10254.
81. Ye Q, Zeng C, Luo C, Wu Y. Ferrostatin-1 mitigates cognitive impairment of epileptic rats by inhibiting P38 MAPK activation. *Epilepsy Behav*. 2020;103(Pt A):106670.
82. Barone FC, Irving EA, Ray AM, et al. SB 239063, a second-generation p38 mitogen-activated protein kinase inhibitor, reduces brain injury and neurological deficits in cerebral focal ischemia. *J Pharmacol Exp Ther*. 2001;296(2):312–321.
83. Bruchas MR, Land BB, Aita M, et al. Stress-induced p38 mitogen-activated protein kinase activation mediates kappa-opioid-dependent dysphoria. *J Neurosci*. 2007;27(43):11614–11623.
84. Singh IN, El-Hage N, Campbell ME, et al. Differential involvement of p38 and JNK MAP kinases in HIV-1 Tat and gp120-induced apoptosis and neurite degeneration in striatal neurons. *Neuroscience*. 2005;135(3):781–790.
85. Sui Z, Fan S, Sniderhan L, et al. Inhibition of mixed lineage kinase 3 prevents HIV-1 Tat-mediated neurotoxicity and monocyte activation. *J Immunol*. 2006;177(1):702–711.
86. Shanware NP, Williams LM, Bowler MJ, Tibbetts RS. Non-specific in vivo inhibition of CK1 by the pyridinyl imidazole p38 inhibitors SB 203580 and SB 202190. *BMB Rep*. 2009;42(3):142–147.
87. Langford D, Oh Kim B, Zou W, et al. Doxycycline-inducible and astrocyte-specific HIV-1 Tat transgenic mice (iTat) as an HIV/neuroAIDS model. *J Neurovirol*. 2018;24(2):168–179.
88. Natarajaseenivasan K, Cotto B, Shanmughapriya S, et al. Astrocytic metabolic switch is a novel etiology for cocaine and HIV-1 Tat-mediated neurotoxicity. *Cell Death Dis*. 2018;9(4):415.
89. Foucault-Fruchard L, Antier D. Therapeutic potential of alpha7 nicotinic receptor agonists to regulate neuroinflammation in neurodegenerative diseases. *Neural Regen Res*. 2017;12(9):1418–1421.
90. Han K, Kim E. Synaptic adhesion molecules and PSD-95. *Prog Neurobiol*. 2008;84(3):263–283.

91. Fernandez E, et al. Arc requires PSD95 for assembly into postsynaptic complexes involved with neural dysfunction and intelligence. *Cell Rep*. 2017;21:679–691.
92. Cao J, Viholainen JI, Dart C, et al. The PSD95-nNOS interface: A target for inhibition of excitotoxic p38 stress-activated protein kinase activation and cell death. *J Cell Biol*. 2005;168(1):117–126.
93. Brenman JE, Chao DS, Gee SH, et al. Interaction of nitric oxide synthase with the postsynaptic density protein PSD-95 and alpha1-syntrophin mediated by PDZ domains. *Cell*. 1996;84(5):757–767.
94. Sultana R, Banks WA, Butterfield DA. Decreased levels of PSD95 and two associated proteins and increased levels of BCl2 and caspase 3 in hippocampus from subjects with amnestic mild cognitive impairment: Insights into their potential roles for loss of synapses and memory, accumulation of Abeta, and neurodegeneration in a prodromal stage of Alzheimer's disease. *J Neurosci Res*. 2010;88(3):469–477.
95. Calabrese F, Riva MA, Molteni R. Synaptic alterations associated with depression and schizophrenia: Potential as a therapeutic target. *Expert Opin Ther Targets*. 2016;20(10):1195–1207.
96. Selkoe DJ. Alzheimer's disease is a synaptic failure. *Science*. 2002;298(5594):789–791.
97. Gong Y, Lippa CF. Review: Disruption of the postsynaptic density in Alzheimer's disease and other neurodegenerative dementias. *Am J Alzheimers Dis Other Demen*. 2010;25(7):547–555.
98. Eugenin EA, King JE, Nath A, et al. HIV-Tat induces formation of an LRP-PSD-95- NMDAR-nNOS complex that promotes apoptosis in neurons and astrocytes. *Proc Natl Acad Sci U S A*. 2007;104(9):3438–3443.
99. Li L-P, Dustrude ET, Haulcomb MM, et al. PSD95 and nNOS interaction as a novel molecular target to modulate conditioned fear: Relevance to PTSD. *Transl Psychiatry*. 2018;8(1):155.
100. Cui H, Hayashi A, Sun H-S, et al. PDZ protein interactions underlying NMDA receptor-mediated excitotoxicity and neuroprotection by PSD-95 inhibitors. *J Neurosci*. 2007;27(37):9901–9915.
101. Khan Z, Lafon M. PDZ domain-mediated protein interactions: Therapeutic targets in neurological disorders. *Curr Med Chem*. 2014;21(23):2632–2641.
102. Chen Y, Wang B, Liu D, et al. Hsp90 chaperone inhibitor 17-AAG attenuates Abeta-induced synaptic toxicity and memory impairment. *J Neurosci*. 2014;34(7):2464–2470.
103. Bustos FJ, Ampuero E, Jury N, et al. Epigenetic editing of the Dlg4/PSD95 gene improves cognition in aged and Alzheimer's disease mice. *Brain*. 2017;140(12):3252–3268.
104. Tripathi P, Singh A, Bala L, Patel DK, Singh MP. Ibuprofen protects from cypermethrin-induced changes in the striatal dendritic length and spine density. *Mol Neurobiol*. 2018;55(3):2333–2339.